End-To-End Optimization of the Layout of a Gamma Ray Observatory

Tommaso Dorigo[1,2,3,4], Max Aehle[1,7], Julien Donini[1,5], Michele Doro[4,2],
Nicolas R. Gauger[1,7], Rafael Izbicki[6], Ann Lee[6], Luca Masserano[6],
Federico Nardi[1,3,4,5], Sidharth S S[8], and Alexander Shen[6]

[1]MODE Collaboration, https://mode-collaboration.github.io/
[2]Istituto Nazionale di Fisica Nucleare - Sezione di Padova, Italy
[3]Universal Scientific Education and Research Network (USERN), Italy
[4]Dipartimento di Fisica e Astronomia "G.Galilei", Università di Padova, Italy
[5]Université Clermont Auvergne, France
[6]Carnegie Mellon University, United States
[7]University of Kaiserslautern-Landau (RPTU), Germany
[8]Indian Institute of Science Education and Research (IISER) Mohali

October 4, 2023

Abstract

In this document we describe a model of an array of water Cherenkov detectors proposed to study ultra-high-energy gamma rays in the southern hemisphere, and a continuous model of secondary particles produced on the ground from gamma and proton showers. We use the model of the detector and the parametrization of showers for the identification of the most promising configuration of detector elements, using a likelihood ratio test statistic to classify showers and a stochastic gradient descent technique to maximize a utility function describing the measurement precision on the gamma-ray flux.

1 Introduction

The optimal choice of layout, characteristics, materials, and information-extraction procedures of a measuring instrument for fundamental science research constitutes a loosely constrained problem, featuring a very large number of free parameters related by non-obvious correlations and constrained by external factors such as budget and science policy. Although typically quite complex, similar problems may sometimes still be tractable by standard means, when an analytical expression of the behavior of the system allows the definition of a likelihood function $\mathcal{L}(\theta) = p(x|\theta)$ given simulated data x, and a solution by minimization of $-\ln \mathcal{L}$ with respect to the modelling parameters θ. When instead the instrument bases its functioning on quantum phenomena such as those governing the

1

interaction of radiation with matter, the optimization problem is typically intractable: the probability $p(x|\theta)$ of observing data x given underlying parameters θ may not be written explicitly. In the latter circumstance, one has access at best to the generating function of the observed data only through forward simulation, a setting commonly referred to as likelihood-free or simulation-based inference [1].

In the latter case discussed above, which is the most common in fundamental physics applications, instrument design is normally informed by extensive studies that sample in s a sparse, discrete manner the space of possible configurations, material and detection process choices, and geometries of the apparatus. Due to the CPU-expensive nature of the computer simulations required to accurately generate the studied phenomena and the interaction of particles with the apparatus, such studies can only probe a very limited number of possible solutions. When the design space spans hundreds (if not thousands) of dimensions this not only becomes highly ineffective in identifying the most advantageous configurations, but also prevents the user from discovering and exploiting hidden structures in the interrelation of the design parameters.

In this work we propose an end-to-end optimization strategy that exploits differentiable programming and a fully continuous model of the physical processes of relevance to address the issue of what is the best layout for the detection elements comprising a planned high-altitude gamma-ray observatory. The main scientific goal of the observatory is the study of gamma-ray fluxes from the southern sky in the TeV-PeV[1] range. Cosmic gamma rays entering Earth's atmosphere generate a shower of secondary particles (electrons, positrons, and photons) whose number grows until it is sustained by enough energy for multiplication to continue, and then dies off when the energy of secondary particles reaches the ionization threshold. By placing a detector of secondary particles at high altitude (above 4,000 m a. s. l.), it becomes possible to reconstruct the energy, direction of incidence, and time of arrival of the primary gamma rays from the observed shower components, and thus contribute to astronomic observations of the gamma-ray sky. For PeV showers, the pattern of secondaries on the ground spans several hundred thousands square meters. Such a large area can be sampled with extended detector arrays. A "fill factor" –the fraction of the ground instrumented by sensitive detection elements– of $5\,\%$ – $80\,\%$ can be achieved in areas of one or a few square kilometers by deploying several thousands of individual detector units. These are particle detectors such as Cherenkov water tanks, scintillators, or resistive plate counters. The number, spacing, and layout of these units, along with their performance, determine the instrument's standard figures of merit: sensitivity, angular and energy resolution, and signal to noise ratio. Noise is mostly represented by hadronic showers, which are of the order of 10^3–10^5 more abundant than gamma rays in the energy range of interest. Their effective discrimination from gamma rays is one of the main challenges of such an experiment.

A maximization of the performance of the above mentioned apparatus can be pursued through the search of the most advantageous geometrical layout of a given number of detection units. The exact definition of a performance metric must reflect the scientific appraisal of different achievable goals, and is beyond the scope of the present technical study; its ingredients are however rather simple to define in terms of attainable precision of the gamma-ray flux, precision of energy and direction measurements, and robustness to modeling systematics. We will address some of the above elements in the definition of a proposed utility metric, which for the time being is meant to be little more than a placeholder. It is however a good starting point as it contains all the mathematical ingredients that play a role in the problem, enabling us to address in detail the issue of how the end-to-end optimization problem can be solved in a differentiable manner. This work is thus entirely within the

---

[1]TeV= Tera Electronvolt = 10^{12} eV. PeV=10^{15} eV.

realm of problems for which some of us have founded the MODE Collaboration[2]. A snapshot of the problems that have so far been attacked with differentiable programming techniques by the MODE collaboration is available at [2].

This document is organized as follows. In Section 2 we briefly introduce the studied detector and its proposed components, focusing on those characteristics that most influence the choices we made in designing an optimization procedure. Section 3 introduces the structure of the optimization pipeline, which can be ideally described as composed of modular blocks performing the loosely connected tasks that convert the physical processes into statistical inference. Section 4 describes the continuous model of atmospheric showers we developed based on full simulation, and the reconstruction of shower parameters by a maximum likelihood technique. In Section 5 We discuss the test statistic we designed to discriminate gamma rays from hadron-induced showers. Section 6 introduces the utility function, which allows us to assess the performance of the geometries as estimated by our model and reconstruction technique. In Section 7 we discuss in detail the optimization procedure. Some preliminary results are shown and discussed in Section 8. We offer some concluding remarks in Section 9.

2   The Gamma-ray Observatory

We will consider in this work a possible future detector which aims to be sensitive to primary cosmic gamma rays in the TeV to PeV range. Its conception is similar to other currently operating instruments, such as the HAWC array in Mexico and the LHAASO array in China, which are both located in the northern hemisphere. The scientific motivation of the considered detector lays in the possibility to study a number of sources in the southern sky, with continuous operation, excellent pointing and energy resolution, and very high discrimination of background from hadronic primaries. In order to achieve sensitivity to TeV-energy showers, such an instrument should be built at high altitude in South America, where it may detect electromagnetic and charged particles of extended atmospheric showers (EASs) generated in the upper atmosphere by the interactions of high-energy gamma rays and protons or light nuclei. The stochastic development of EASs is well described by the formalism of Rossi and Greisen [3] and depicted in Fig. 1. Electromagnetic showers and sub-showers develop through the processes of pair production and bremsstrahlung, while hadronic showers involve more complex interactions including the generation of pions and kaons and their subsequent decays. The multiplication processes cease when electrons reach a critical energy threshold and hadrons lose the ability to generate further $2 \rightarrow$ many strong interactions, after which secondaries get progressively absorbed and the shower dies off. If a detector is placed before that point, whose location depends on the primary particle energy and direction, it has a chance to sample the shower's particle and radiation content and allow inference of the primary particle type, direction, energy, and arrival time, effectively making the instrument a 'telescope'. An EAS develops laterally so that on the ground an area of several hundreds of meters of radius (up to thousands of meters) is hit by particles for the duration of a few nanoseconds.

The observatory we consider may consist of several thousand detector units. Although there are a number of detection technologies that can be used to measure charged and neutral particles, EAS arrays mostly use Cherenkov water tanks, which detect the Cherenkov light generated by high-energy particles in purified water through one or more photosensors. This technique is *e.g.* used by HAWC [4], LHAASO [5], and the Pierre Auger Observatory [6], among others. Alternatives

---

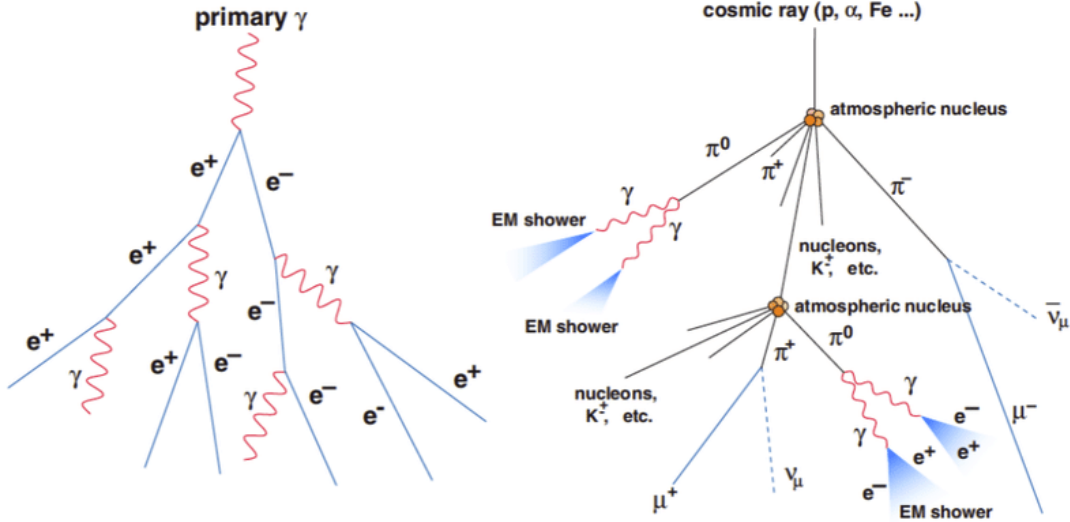[2]Web site: https:
mode-collaboration.github.io

Figure 1: Electromagnetic and hadronic showers

include the deployment of photodetectors in excavated ponds; there are also studies for detector units constituted by submerged bladders submerged below the surface of a lake. In addition, or in synergy with water tanks, different detector units based on Resistive Plate Chambers or Scintillator planes are also in use [7].
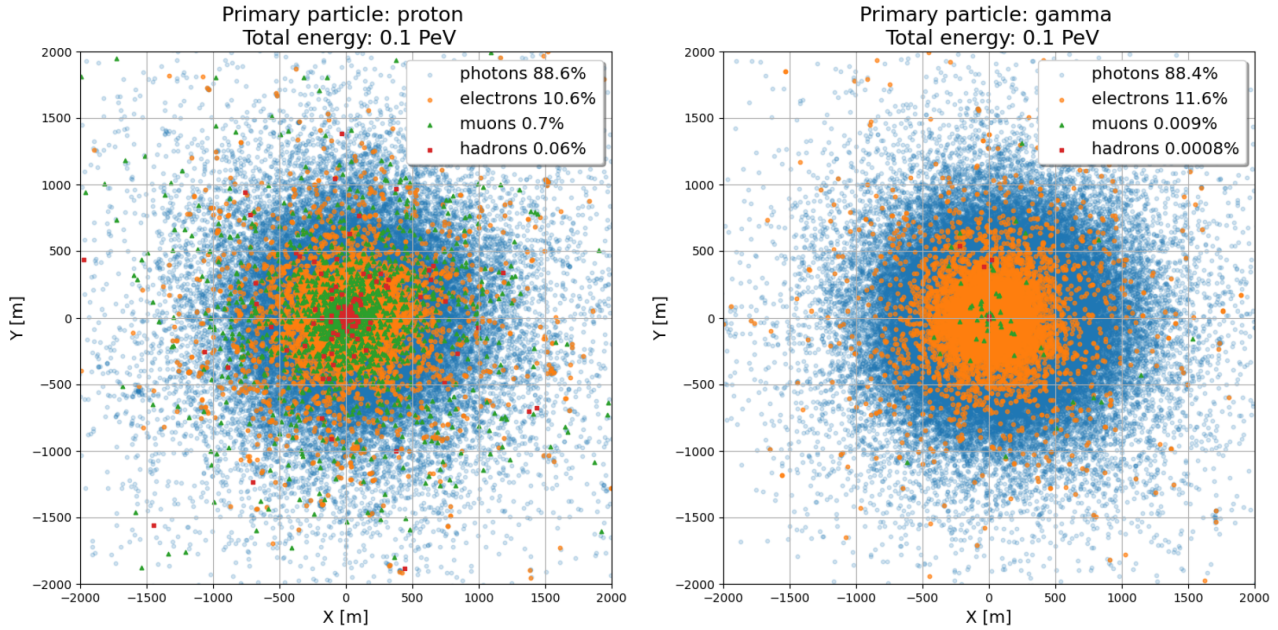

Figure 2: Radial distribution of secondary particles on the ground, originated at 4.8 km altitude by a 100 TeV proton (left) or photon shower (right).

On the ground, mostly electrons and positrons (collectively electrons hereafter) and secondary gamma rays can be observed. Hadronic showers, besides containing electromagnetic sub-showers produced by early energetic neutral pions, also generate muons and heavier particles; see Fig. 1.

The size of the particle footprint on the ground largely depends on the proximity of the shower maximum development, which in turns depends on the energy of the primary (the larger the primary energy, the closer the shower maximum is to the ground) and its angle of incidence from the vertical (hereafter, the polar angle θ). The radial distribution can extend to a few hundred meters for showers of hundreds of GeV, to more than a km for PeV showers (see Fig. 2 and Fig. 3).
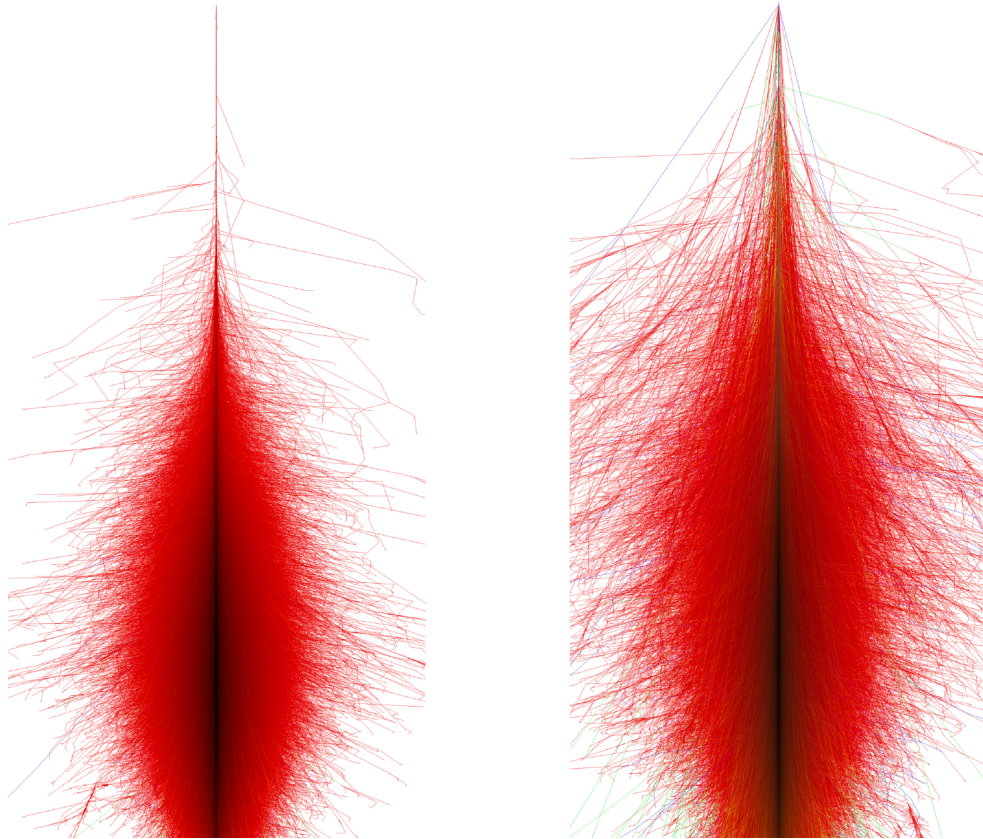

Figure 3: Lateral development of 100 TeV showers from a primary photon (left) and proton (right). Source: Corsika web page[8]

A typical configuration for the layout of the water tanks should address the need to separately count the collective number of electrons and photons reaching the ground, as well as the number of muons and heavier particles. Muons in particular are very rare in gamma ray-originated showers, especially for gamma rays at lower energy, and they thus constitute a powerful discriminator of hadron backgrounds; for PeV gamma rays, muon-antimuon pair production by the primary particle starts to be significant, and is an additional source of confusion. Due to their higher penetration power, muons can cross the entire atmosphere and reach the ground, thus constituting one of the main components of hadronic showers. Inside a water tank, muons also generate Cherenkov light. Water tanks may be able to distinguish these particles from electrons and photons if they are segmented vertically in two parts, where the upper part absorbs the light generated by the e.m. component; due the limited range of electrons in water, only muons get through to the lower part of the tank and produce Cherenkov light there. Although that possibility has not yet been explored, it is in principle possible to distinguish the pattern of muon radiation (which is more compact in time and shape) provided that accurate timing and multiple photosensors are in place. Optimization studies of these designs may enable finding the right compromise between cost, logistics, and performance

of the units.

A loosely connected issue to the one of the most performant unit design concerns the arrangement of the units on the ground. The footprint of energetic air showers may span several hundred meters or even kilometers at the considered height above sea level, and the capability of the array to appropriately measure the energy of the primary particle in the low-energy range of interest to some specific measurements (tens-hundreds of GeV) requires the collection of as large a fraction of the collective signal of particles on the ground as possible; this mandates that tanks be laid out as tightly packed as possible –*i.e.* with a fill factor of 50 % or more. On the other hand, in order to be sensitive to the very low flux of photons of extremely high energy (1 PeV and above), the total instrumented area (including the void between units) needs to be maximized with detectors distributed with a low fill factor and well spaced from one another, meeting cost constraints. However, too low fill factors will hinder both a precise energy reconstruction and a successful separation of hadron backgrounds, whose rate at those high energies exceeds that of gamma rays by a factor of 10^4 and above.

2.1 Detector unit design

For our study we will consider a generic water tank design, constituted by a 1.9m radius cylinder filled with a body of water watched by one or more photomultiplier tubes, in such a way to allow for effective discrimination of the electromagnetic and muonic component of incident secondary particle flux from the atmospheric shower.

For the remainder of this work we are not interested in the design details more than the bare-bones description provided above, as their inclusion in the optimization procedure would be premature. We further assume full efficiency for particle detection: that is, a probability of 1.0 that units detect and correctly identify secondary particles. These assumptions are certainly not valid, but they factor out of the procedure and have limited impact in the variation of the utility with respect to a variation of the layout of tanks on the ground.

2.2 Array Specification

A number of possible arrangements of several thousand detector units on the ground may be considered. They should in general share a radial symmetry and possibly a higher fill factor in the core, with a smaller one at larger radii. At multi-GeV energies the flux of primaries is high, but their footprint on the ground has a limited extension and the precise reconstruction of shower parameters is limited by the number of detectable particles, which is much smaller than for TeV- and PeV-energy showers. At TeV energies the rate of events is still relatively high, and in order to keep the signal to noise ratio large enough for effective discrimination one should be able to sample a fraction as high as possible of the shower footprint. A tightly packed layout of detection tanks produces an effective shield from laterally entering electrons and photons: each detector, whose height from the ground may be of the order of 1.5-3 meters, can effectively prevent the soft secondaries component from penetrating on nearby units sideways and reaching into the bottom of the traversed tank –a phenomenon producing a confounding background to the hard component of the showers. On the other hand, the rationale of a further extended area instrumented at lower fill factor is to allow for the highest effective instrumented area, to be sensitive to very rare ultra-high-energy (PeV) photons whose rate per unit area is smaller than for lower energies. In case of the sparse outer array, a rejection of lateral through-going particles can be still obtained with different solutions all connected to

shielding the lower chamber of the tank (in case of double-chamber tanks) either by water or ground. That problem does not exist in case of single-chamber tanks.

The two requirements of low-energy precision and high-energy flux maximization are in tension with one another, and they already indicate that an optimization of the layout requires a precise definition of the relative scientific importance of the many objectives of the observatory's scientific program. We are not deterred by this complication, as we are aware of similar situations in other branches of experimental physics where compromises are routinely struck between a large number of conflicting demands. The classical example is the trigger menu of a hadron collider experiment, where the limited bandwidth available for event storage demands a very high rejection factor (of the order of 10^4 and above); events of interest for different physics measurements and searches are thus subjected to restrictions in the data-acquisition rate, based on painful but routinely taken decisions on the rate budget of each channel of interest.

2.3 Full simulation datasets

Atmospheric showers may be accurately generated via the publicly available `CORSIKA` software [9]. The software simulates the full development of the particle showers, and, once the detector elevation above sea level is fixed, stores all ground particle information including particle position, type, momentum, direction and direction. This step of the simulation is quite CPU- and storage-expensive, with increasing time and storage required as the primary energy increases. The simulations we employed to obtain a parametric model (Sec. 3) are detailed in Table 1 below. In all cases listed there, the detector altitude has been fixed at 4,800 m a.s.l. In general, the higher is the altitude of the detector, the higher will be the sensitivity at the lowest energies of primary showers. We make use of simulation of showers with energy between 0.1 PeV and 10 PeV produced by INFN at the Italian CNAF data center [10].

	ID	Energy	Angle	Events
1	γ	0.1/0.3/1./3. PeV	20°/40°	10k
2	γ	0.1-10 PeV	0°-65°	100k
3	p	0.1-10 PeV	20°/40°	200k
4	p	1.0-10 PeV	0°-65°	200k

Table 1: Corsika-produced datasets of proton and photon showers used in the present work.

3 The modeling pipeline

The contrasting requirements mentioned in the previous section may lead one to consider layouts that share as a common feature a dense core and an extended region more sparsely populated. Evaluation in precise quantitative terms the relative benefit of any proposed layout, for various astrophysics cases of interest may be produced with full simulation.

Here we consider a set of $N_{\rm det}$ water Cherenkov detectors all of the same characteristics: cylinders of radius $R = 1.9$ m with axes oriented along the vertical z direction, filled with water and instrumented with light-sensitive photodetectors in an arrangement capable of discriminating light signals produced by the soft component (photons, electrons, and positrons) from signals produced by

muons. We do not consider the details of the individual tanks, leaving that part of the optimization problem separated from the one of finding the most proficuous geometry of N_{det} units on the ground.

In order to simplify the geometry optimization problem, we decouple it from the detector optimization part by operating a number of assumptions. We assume that each detector is capable of detecting with 100% efficiency particles hitting their top cross-sectional area, thus freeing ourselves from the arduous task of modeling the direction of secondaries on the ground as well as modeling their detection efficiency. We also assume that there is no uncertainty in the number of detected particles with energy above a given cutoff, within the time interval when secondaries from a cosmic showers cross the detector array. Finally, a time resolution of 1 ns is assumed on the signal of particles detected by each unit. With the above assumptions, the set of detecting units is thus specified solely by the position of the center of each unit on the ground, $(x_i, y_i), i = 1...N_{\text{det}}$.

By the simulation of a large number of showers and the reconstruction of their parameters, it is possible to mimic a full-fledged measurement under any hypothesis for the unit layouts, obtaining a relative appraisal of different configurations: it is a simple exercise once a reconstruction method and a utility function are specified. The more principled question, however, concerns the investigation of the way more high-dimensional space of all possible configurations of N_{det} detectors. As a detector position is specified by its ground coordinates $(x_i, y_i), i = 1...N_{\text{det}}$, the space of configurations lives in $\mathcal{R}^{2N_{\text{det}}-3}$, accounting for the azimuthal symmetry of the problem. So, $e.\,g.$, the layout of three units involves the choice of three real parameters: by setting the first unit in $(0,0)$, the second can be set at $(x_2, 0)$ without loss of generality; the third can then be specified by (x_3, y_3), when y_3 can be chosen in the positive semi-axis without loss of generality. With a reference number of, $e.g.$, 6000 units to be deployed, the space of possibilities grows prohibitively large and impossible to probe with discrete methods.

The task of writing an optimization pipeline that scans the large parameter space with differentiable programming can be addressed only if one endows oneself with a parametrized approximation of the density of particles on the ground as a function of the distance from the shower axis, resulting from a cosmic ray shower of given energy E and polar angle θ. Ideally this should be available in closed form for both gamma and proton-originated showers (the background to discriminate against), and for the particle types to which the detectors are differently sensitive: electrons, positrons, and photons (which can be in first approximation be considered together, due to their similar behaviour in interacting with water at energies much above the critical energy E_{crit}, which is of $76.2\,\text{MeV}$ for positrons and $78.3\,\text{MeV}$ for electrons [11]), and muons. As atmospheric showers arising from high-energy primaries involve a number of complex stochastic processes, precise parametrizations are difficult to produce; yet even a mildly inaccurate choice may be able to successfully inform a continuous scan of the parameter space, if a full simulation is then used to validate the results in the vicinity of interesting configuration points.

We use `Corsika` [9] simulations of gamma and proton showers at different energies (from $100\,\text{GeV}$ to $10\,\text{PeV}$) described in Sec. 2.3 to extract a model of the density of secondary particles on the ground as a function of the distance from shower axis. The resulting model is the basis of the optimization pipeline which is described in what follows.

1. The starting point is the generation of an initial ground configuration of N_{det} detector units, $(x_i, y_i)_{i=1,...N}$.

2. A set of gamma and proton showers are simulated with an intersection of the shower axis with the ground at a position (X_0, Y_0) randomly chosen within a region exceeding on all sides the initial footprint assumed for the detector tanks, such that showers at the edge of this region have a negligible probability of being detected by the array. We find that $1.5\,\text{km}$ of radial

extension is sufficient for this task, and 2 km are a safer but more CPU consuming choice (see *infra*, Sec. 5.3); triggering requirements may further reduce this area. A given shower energy E and polar angle θ, the position of the shower center on the ground, together with the azimuthal angle ϕ defined as the angle between the horizontal component of the shower axis and the positive x direction, determine an estimate of the average number of particles of different kinds that will hit the sensitive area of each of the N_{det} detector units. These numbers can be sampled from Poisson distributions of means equal to the estimated averages.

3. Through a likelihood maximization, estimates of the shower parameters are obtained by considering the true value of the parameters of the model, and the number of particles detected for each species in each tank under, for the time being, the assumption that tanks have 100 % detection efficiency and perfect discrimination power between the various particle species. The likelihood is maximized under either hypothesis (gamma or proton) for each shower, regardless of the true primary particle species.

4. The obtained likelihood values, maximized over shower parameters E, θ, ϕ, X_0, and Y_0, are used to compute a likelihood ratio test statistic TS for each generated shower. The sampling of a large number of showers of different parameters allows to construct a Probability Density Function (PDF) of TS for both hypotheses.

5. A new batch of gamma and proton showers is generated, and a distribution of TS values obtained. This is fit as the sum of the two distributions, and an estimate of the uncertainty on the fraction of gammas in the batch is extracted by use of the Rao-Cramer-Frechet bound [12].

6. Using the uncertainty on the gamma fraction, a utility function is computed to reflect as closely as possible the goals of the experiment. A simple proxy to sensitivity of the detector array to signals at high energy may be a properly weighted sum of the inverse of the relative uncertainty in the flux of gammas in a batch of showers, where the batch represents the data collectable in a given time interval.

7. A propagation of derivatives then allows to extract the derivative of the utility function U over displacements $(\delta x_i, \delta y_i)_{i=1,...,N_{det}}$ for each of the N_{det} detector units. These are used to update the detector positions.

8. The cycle can be continued by generating a new set of gamma and proton showers and deriving new PDF of TS, then fitting a batch of showers and recomputing U.

The pipeline described above is summarized in Fig. 4. It allows to converge to layouts that optimize the utility function, focusing on the precision of the gamma flux. Of course, more complex utility functions than the one described above could be conceived, to model the real objectives of the wide scientific program of the discussed observatory. This modeling task has not yet been attempted; we only explored the addition of an integrated energy resolution term to the utility function (see Sec. 6). In the near future the code will be expanded to improve the way it represents the full inference-extraction procedures, with a view to providing useful input to the collaboration on the most advantageous layouts of tanks on the ground. The relative gains of those layouts over baseline ones can then be appraised by exploiting full simulation of atmospheric showers and detection of secondaries by the detector units.

In parallel, a parametrization of the detection of particles of different species, their energy distribution, the tank efficiency, and backgrounds may be included in the pipeline, improving the precision
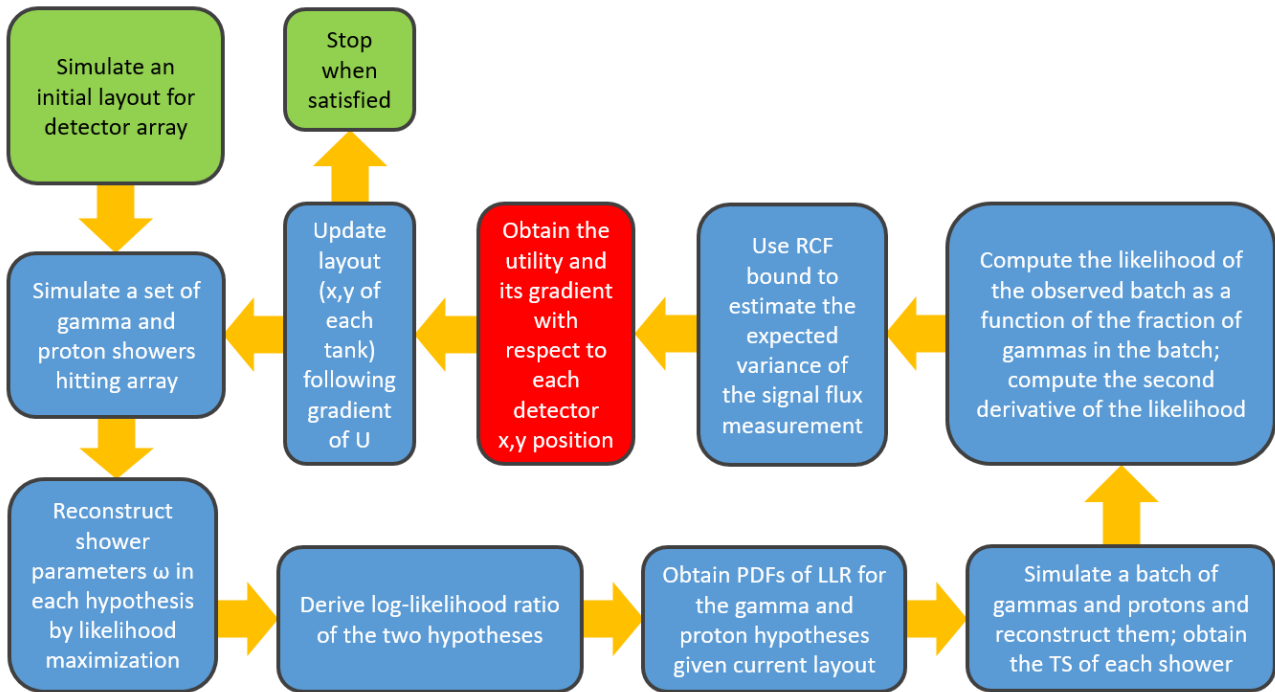
Figure 4: Block diagram for the optimization of the detector array.

.

of the model. In the following section we describe the modeling of each functional block in the pipeline we summarized above.

4 Shower Parametrization and Reconstruction

4.1 Continuous Parametrization of Secondaries from Photon and Proton Showers

The simulated atmospheric showers mentioned in Sec. 3 are used to extract a simple parametric model that determines, as a function of the radius from the shower axis and altitude of 4800 m, the density of secondaries of different species possessing momenta above a suitable threshold, given a primary particle identity (proton or photon), energy E, and polar angle θ. For the time being we do not focus on a precise modeling of the individual detection of secondary particles in the tanks or their energy release, and we therefore choose an energy threshold (10 MeV) such that it roughly correspond to a baseline probability of detection by Cherenkov tanks of similar properties to those currently considered by the collaboration.

We do not make any attempt to model subtle effects that modify the density profile of showers as a function of radius, such as clumpiness of proton showers in the number of muons on the ground or other properties which, while potentially very useful to discriminate the identity of the primary particle, can be dealt with in a more detailed study with the full simulations.

We further simplify our modeling task by computing a sum of the flux of electrons, positrons and photons, by reasoning that their signal in the Cherenkov tanks is topologically similar, and produce a single set of distributions depending on primary identity, energy and polar angle; we also sum together positive and negative muon fluxes into a second set of distributions. For modeling purposes we initially divide the primary energy into 20 logarithmic-equally-spaced energy bins on the 0.1 PeV - 10 PeV energy range, and primary polar angles into 4 bins in the 0 - 65 degrees angle. These are thus 320 distributions: 80 for electromagnetic particles from gamma primaries, 80 more for muons from gamma primaries, and 160 more of the same kinds from proton primaries.

We obtain fluxes of particles into the detector as a function of the radial distance from the shower axis by projecting on the transversal plane their ground position, and normalizing their flux to particles per square meter. We assign Poisson uncertainties on their number after averaging out many showers simulated in each energy and polar angle bin (see Table 2). Then we proceed to fit these fluxes with the following functional form:

$$\frac{dN^{\mu,\gamma}(E_\gamma|\theta_\gamma)}{dR} = p_0^{\mu,\gamma}(E_\gamma|\theta_\gamma) \cdot \exp\left(-p_1^{\mu,\gamma}(E_\gamma|\theta_\gamma)R^{p_2^{\mu,\gamma}(E_\gamma|\theta_\gamma)}\right) \tag{1}$$

$$\frac{dN^{e,\gamma}(E_\gamma|\theta_\gamma)}{dR} = p_0^{e,\gamma}(E_\gamma|\theta_\gamma) \exp\left(-p_1^{e,\gamma}(E_\gamma|\theta_\gamma)R^{p_2^{e,\gamma}(E_\gamma|\theta_\gamma)}\right) \tag{2}$$

$$\frac{dN^{\mu,p}(E_p|\theta_p)}{dR} = p_0^{\mu,p}(E_p|\theta_p) \exp\left(-p_1^{\mu,p}(E_p|\theta_p)R^{p_2^{\mu,p}(E_p|\theta_p)}\right) \tag{3}$$

$$\frac{dN^{e,p}(E_p|\theta_p)}{dR} = p_0^{e,p}(E_p|\theta_p) \exp\left(-p_1^{e,p}(E_p|\theta_p)R^{p_2^{e,p}(E_p|\theta_p)}\right) \tag{4}$$

We study the distribution of these sets of parameters as a function of 20 values of the primary particle energy, for each of four values $\theta_0 \div \theta_3$ of the polar angle (centers of four bins in the $[0° \div 65°]$ range), and interpolate them in order to obtain a prediction of the value of each parameter for any value of E and for each of the four θ values. This is done by fitting the parameters p_0, p_1, and p_2 of each of the four theta values as a function of the logarithm of the primary particle energy:

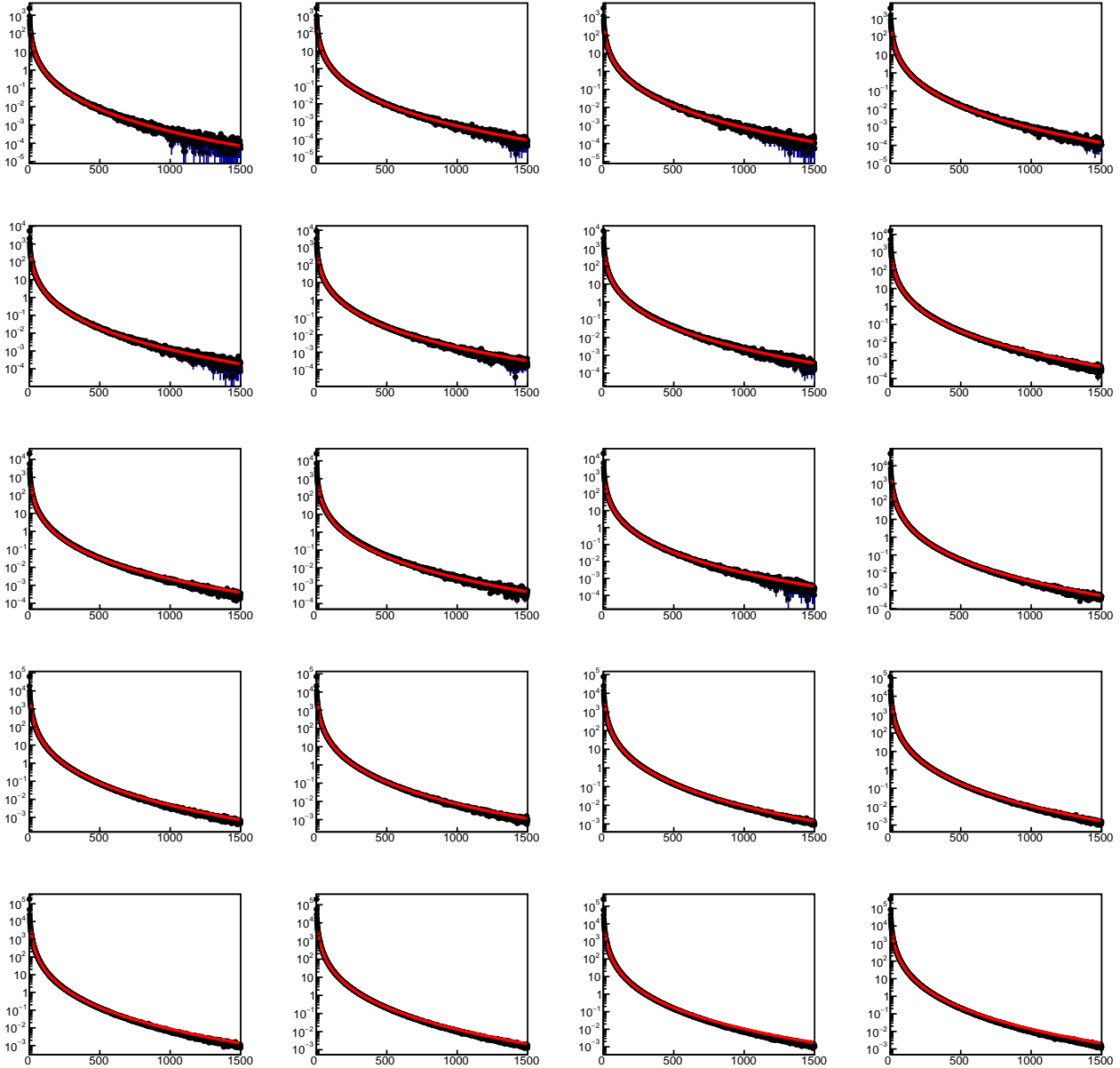$$p_i(E|\theta_j) = q_{i0}(\theta_j) \exp\left[q_{i1}(\theta_j)[\ln(E/E_0)]^{q_{i2}(\theta_j)}\right] \tag{5}$$

Figure 5: Combined flux of electrons and photons (with ground energy above 10 MeV) from photon primaries of polar angle θ_γ in the $[0, 16.25]$ degrees range, for energies of 100 TeV (top left) to 10 PeV (bottom right). The model is overlaid in red to the distributions.

Parameters q_{ij} are tabulated in Table 2 and Table 3. The sets of parameters p and q are redundant, but their simultaneous presence simplifies the convergence of bulk fitting of the histograms in the case of the high-statistics distributions of electrons plus photons, $dN_{e,\gamma}/dR$. For fits to muon fluxes we obtain sufficiently good convergence by fixing all p_1 parameters to 1.0 (and consequently the corresponding q_{i1} parameters are set to $(1, 0, 0)$). The procedure to turn the sets of parameters into a continuous model is performed as follows:

1. For each of the 20 studied values of shower energy we determine the parameters $\alpha, \beta, \gamma, \delta$ of the cubic function that reproduces the values of each of the p_0, p_1, p_2 parameters at the four available values of polar angle: *e. g.*, for the first parameter p_0 required to compute the flux of
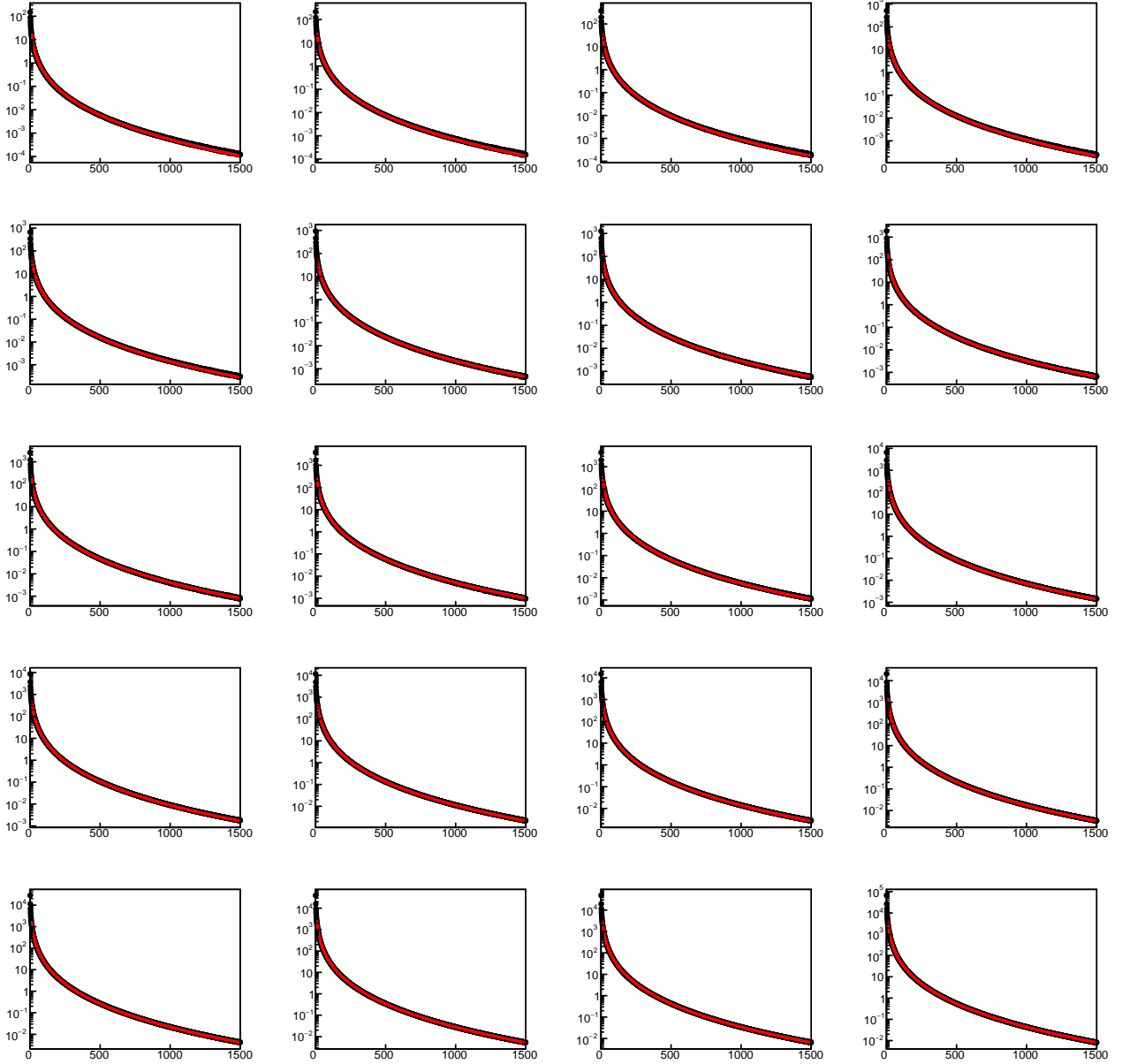
Figure 6: Combined flux of electrons and photons (with ground energy above 10 MeV) from proton primaries of polar angle θ_γ in the $[32.5, 48.75]$ degrees range, for energies of 100 TeV (top left) to 10 PeV (bottom right). The model is overlaid in red to the distributions.

muons from proton primaries we write

$$\alpha(E_i) + \beta(E_i)\theta_j + \gamma(E_i)\theta_j^2 + \delta(E_i)\theta_j^3 = p_0^{\mu,p}(\theta_j|E_i) \tag{6}$$

with $j = 1, 2, 3, 4$ spanning the four bins in polar angle, and

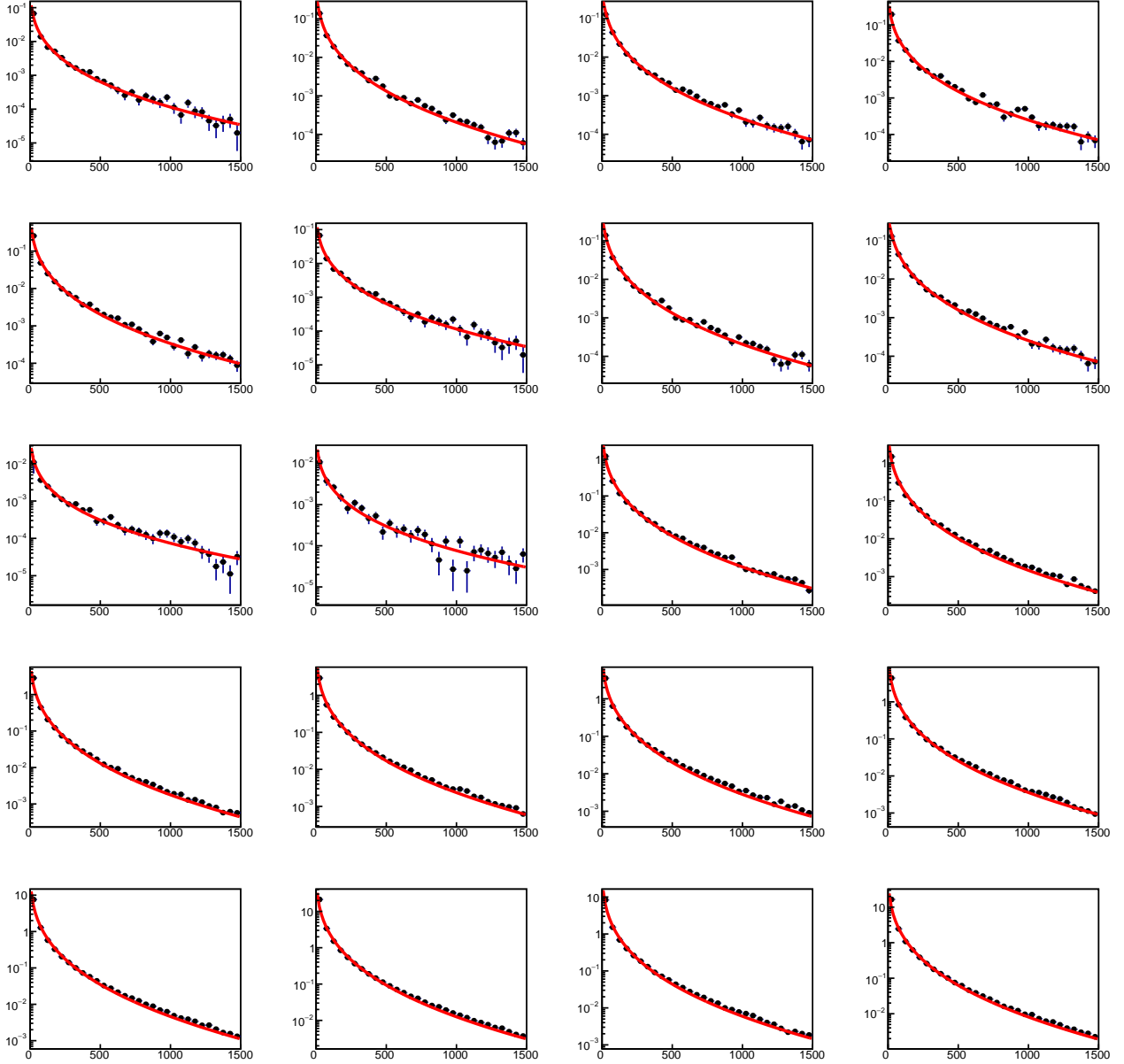$$\theta_j = \frac{j - 0.5}{4}\left(\pi\frac{65}{180}\right) \tag{7}$$

13

Figure 7: Flux of muons (with ground energy above 10 MeV) from photon primaries of polar angle θ_γ in the $[16.25, 32.5]$ degrees range, for energies of 100 TeV (top left) to 10 PeV (bottom right). The model is overlaid in red to the distributions.

and with

$$E_i = \exp\left[(\ln 10 - \ln 0.1)\frac{i + 0.5}{20} + \ln 0.1\right] \tag{8}$$

where we make explicit that we studied polar angles up to 65 degrees of inclination from the vertical, and energies in the range 0.1 PeV - 10 PeV. The above calculation is performed by computing:

14
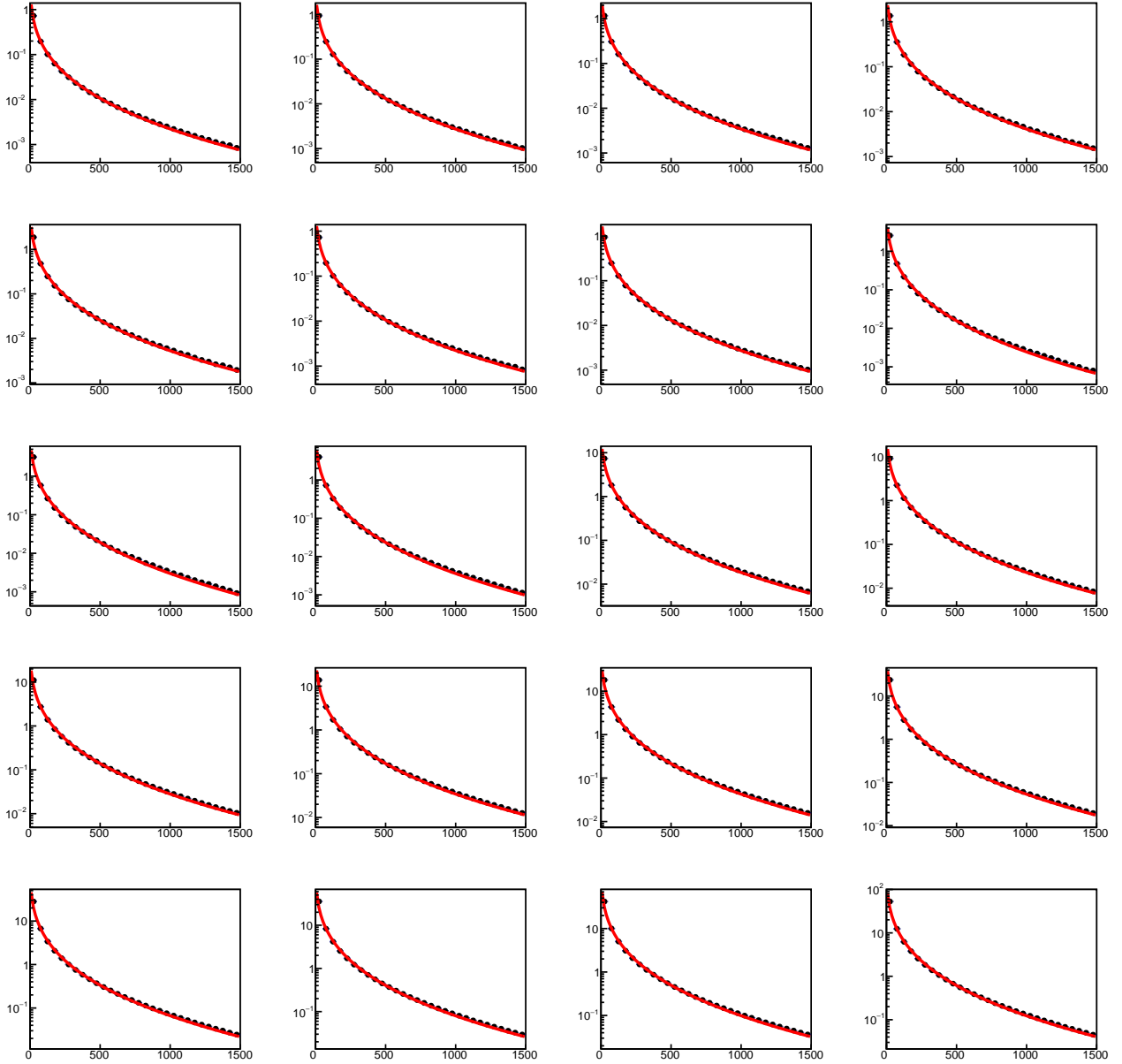
Figure 8: Flux of muons (with ground energy above 10 MeV) from proton primaries of polar angle θ_γ in the $[48.75, 65]$ degrees range, for energies of 100 TeV (top left) to 10 PeV (bottom right). The model is overlaid in red to the distributions.

$$
\begin{pmatrix}
\alpha(E_i) \\
\beta(E_i) \\
\gamma(E_i) \\
\delta(E_i)
\end{pmatrix}
= A^{-1}
\begin{pmatrix}
p_0^{\mu,p}(\theta_1)_i \\
p_0^{\mu,p}(\theta_2)_i \\
p_0^{\mu,p}(\theta_3)_i \\
p_0^{\mu,p}(\theta_4)_i
\end{pmatrix}
\tag{9}
$$

where A is the 4×4 matrix whose k-th row and j-th column contains the $(j-1)$-th power of k:

15

$$A = \begin{pmatrix} 1 & 1 & 1 & 1 \\ 1 & 2 & 4 & 8 \\ 1 & 3 & 9 & 27 \\ 1 & 4 & 16 & 64 \end{pmatrix}$$

2. For each flux parameter $(p_i^{\{\mu,e\},\{\gamma,p\}}(E,\theta))$, the parameters defining the cubic functions are then computed for 100 values of θ and 100 values of E evenly spaced in the relevant ranges of the two variables, and stored in a 100×100 lookup table. We may then compute each flux parameter at any real value of energy and polar angle by linear interpolation from the known grid values.

3. Along with tables containing parameter values, separate 100×100 tables are built to contain values of the parameters derivatives with respect to energy and polar angle. These are needed for calculation of derivatives of the fluxes (see *infra*, Sec. 4.2).

By the above procedure we obtain a continuous model of the flux of each secondary particle species for each primary particle of energy E and polar angle θ. The typical precision in the flux produced by the parametrization is better than 10 % in the shower axis, and better than 20 % at radii of 1.5 km from the shower axis, where particle fluxes have typically decreased down to a part in 100,000 or less of the central flux. For gamma showers, fluxes of electrons and gammas (resp. muons) overall have a standard deviation from the model equal to 15.6 % (resp. 18.9 %). For proton showers, standard deviations are of 3.8 % for electron plus gamma fluxes (resp. 8.4 % for muon fluxes). We deem this precision more than sufficient for the scope of the present work. Sample radial profiles of the particle densities along with extracted parametric fits are also shown in Fig. 5 and Fig. 7 (Fig. 6 and Fig. 8) for photon (proton) primaries, respectively.

4.2 Derivatives of the Fluxes

In order to compute the gradient of the utility function in the gradient descent routine discussed above, we are going to need to compute derivatives of the fluxes as a function of shower parameters. The calculation is straightforward but tedious. We provide below its essential results.

The derivative of the flux with respect to the distance R of a detector unit from the shower center is straightforward:

$$\frac{d\left(dN/dR\right)}{dR} = -p_1 p_2 R^{p_2-1} \frac{dN}{dR} \tag{10}$$

The flux derivative with respect to shower energy E, however, is more contrived. We get it from:

$$\frac{d\left(dN/dR\right)}{dE} = \left(\frac{1}{p_0} \frac{dp_0}{dE} - R^{p_2} \frac{dp_1}{dE} - p_1 R^{p_2} \ln R \frac{dp_2}{dE} \right) \frac{dN}{dR} \tag{11}$$

for which we need interpolated values of the derivatives of flux parameters $\frac{dp_i}{dE}$ ($i = 1, 2, 3$), already obtained as discussed in the previous subsection.

Finally, the derivative of the flux with respect to polar angle can be obtained as:

$$\frac{d(dN/dR)}{d\theta} = \left(\frac{1}{p_0} \frac{dp_0}{d\theta} - R^{p_2} \frac{dp_1}{d\theta} - p_1 R^{p_2} \ln R \frac{dp_2}{d\theta} - p_1 p_2 R^{p_2-1} \frac{dR}{d\theta} \right) \frac{dN}{dR} \tag{12}$$

which also makes use of the lookup tables for the derivatives of the flux parameters, $dp_i/d\theta(i = 1, 2, 3)$.

Parameter	p_0 (m^{-1})	p_1	p_2
$q_0(\theta_0)_{e,\gamma}$	36117.1	0.172385	1.21588
$q_0(\theta_1)_{e,\gamma}$	24130.6	0.154078	1.23513
$q_0(\theta_2)_{e,\gamma}$	1730.82	0.626387	0.82250
$q_0(\theta_3)_{e,\gamma}$	83.7947	0.958974	0.71986
$q_1(\theta_0)_{e,\gamma}$	3.29423	0.057859	1.73547e-3
$q_1(\theta_1)_{e,\gamma}$	3.00016	0.069276	3.37280e-4
$q_1(\theta_2)_{e,\gamma}$	2.70469	0.041916	3.68160e-4
$q_1(\theta_3)_{e,\gamma}$	2.22895	0.116381	-3.67932e-3
$q_2(\theta_0)_{e,\gamma}$	0.252659	-3.23064e-3	0.48205e-4
$q_2(\theta_1)_{e,\gamma}$	0.266636	-4.94512e-3	1.25588e-4
$q_2(\theta_2)_{e,\gamma}$	0.249405	-6.40193e-5	-0.47208e-4
$q_2(\theta_3)_{e,\gamma}$	0.262290	-4.43699e-3	1.73817e-4
$q_0(\theta_0)_{\mu,\gamma}$	-358.593	0.151459	1.17910
$q_0(\theta_1)_{\mu,\gamma}$	-740.388	0.107846	1.31133
$q_0(\theta_2)_{\mu,\gamma}$	-113.901	0.064268	1.46762
$q_0(\theta_3)_{\mu,\gamma}$	-116.403	0.013792	1.90919
$q_1(\theta_0)_{\mu,\gamma}$	1	0	0
$q_1(\theta_1)_{\mu,\gamma}$	1	0	0
$q_1(\theta_2)_{\mu,\gamma}$	1	0	0
$q_1(\theta_3)_{\mu,\gamma}$	1	0	0
$q_2(\theta_0)_{\mu,\gamma}$	0.325954	-0.00141329	1.07998e-4
$q_2(\theta_1)_{\mu,\gamma}$	0.321244	-0.00156709	1.17792e-4
$q_2(\theta_2)_{\mu,\gamma}$	0.309210	0.00104322	-0.18057e-4
$q_2(\theta_3)_{\mu,\gamma}$	0.289677	0.00248633	-0.87118e-4

Table 2: Parameters of the energy dependence of parameters p_i for the flux model of photon-originated secondaries. From top to bottom: e.m. particles from gamma showers; muons from gamma showers. The four $\theta_0 \div \theta_3$ values are the centers of four bins in the $[0° \div 65°]$ polar angle range where primaries have been generated with `corsika`, as discussed *supra*.

4.3   Reconstruction of Shower Parameters

Given a layout of N_{det} Cherenkov tanks, specified by their $(x_i, y_i)_{i=1...,N_{\mathrm{det}}}$ positions on the ground, and the assumptions we have discussed above, the data that the array collects upon being hit by an atmospheric shower can be specified in the form of $4N_{\mathrm{det}}$ numbers: the number of e.m. (muon) secondaries $N_{e,i}$ ($N_{\mu,i}$, respectively) that reach detector i, and the time of arrival at detector i of the e.m. (muon) component $T_{e,i}$ ($T_{\mu,i}$, respectively), with $i = 1...N_{\mathrm{det}}$.

Once we define the parametrization of the differential fluxes of the two kinds of particles on the ground as a function of distance from the shower axis is defined as described above, assuming no uncertainty on the model itself, we can write an expression for the probability of observing the set of $4N_{\mathrm{det}}$ variables, under the hypothesis that the shower is originated by a gamma or proton primary:

$$\mathcal{L}^{\gamma}(\lambda_e, \lambda_\mu, t_{e,i}^{\mathrm{exp}}, t_{\mu,i}^{\mathrm{exp}}) = \prod_i P(N_{e,i}|\lambda_{e,i}^{\gamma}) P(N_{\mu,i}|\lambda_{\mu,i}^{\gamma}) G(T_{e,i} - t_{e,i}^{\mathrm{exp}}) G(T_{\mu,i} - t_{\mu,i}^{\mathrm{exp}}) \tag{13}$$

$$\mathcal{L}^{p}(\lambda_e, \lambda_\mu, t_{e,i}^{\mathrm{exp}}, t_{\mu,i}^{\mathrm{exp}}) = \prod_i P(N_{e,i}|\lambda_{e,i}^{p}) P(N_{\mu,i}|\lambda_{\mu,i}^{p}) G(T_{e,i} - t_{e,i}^{\mathrm{exp}}) G(T_{\mu,i} - t_{\mu,i}^{\mathrm{exp}}) \tag{14}$$

Parameter	p_0 (m^{-1})	p_1	p_2
$q_0(\theta_0)_{e,p}$	9.61560	5.20551	0.364469
$q_0(\theta_1)_{e,p}$	9.28613	4.84781	0.378406
$q_0(\theta_2)_{e,p}$	8.30776	4.28549	0.394419
$q_0(\theta_3)_{e,p}$	6.06557	3.95115	0.370725
$q_1(\theta_0)_{e,p}$	3.00069	0.0715927	-1.90026e-4
$q_1(\theta_1)_{e,p}$	2.86508	0.0677157	-4.22523e-4
$q_1(\theta_2)_{e,p}$	2.65306	0.0549206	-5.74074e-4
$q_1(\theta_3)_{e,p}$	2.61631	0.0606328	-1.55515e-3
$q_2(\theta_0)_{e,p}$	0.245223	-2.33057e-3	4.04411e-5
$q_2(\theta_1)_{e,p}$	0.247950	-2.24902e-3	4.35953e-5
$q_2(\theta_2)_{e,p}$	0.250321	-1.71418e-3	3.40669e-5
$q_2(\theta_3)_{e,p}$	0.239306	-1.15019e-3	2.81104e-5
$q_0(\theta_0)_{\mu,p}$	3.29812	1.49020	0.532621
$q_0(\theta_2)_{\mu,p}$	3.20693	1.43384	0.542787
$q_0(\theta_2)_{\mu,p}$	2.82742	1.26128	0.573445
$q_0(\theta_3)_{\mu,p}$	1.82703	0.89117	0.652063
$q_1(\theta_0)_{\mu,p}$	1	0	0
$q_1(\theta_1)_{\mu,p}$	1	0	0
$q_1(\theta_2)_{\mu,p}$	1	0	0
$q_1(\theta_3)_{\mu,p}$	1	0	0
$q_2(\theta_0)_{\mu,p}$	0.324353	3.37751e-4	-1.30596e-6
$q_2(\theta_1)_{\mu,p}$	0.322256	2.99934e-4	-1.06650e-6
$q_2(\theta_2)_{\mu,p}$	0.316132	2.93557e-4	-1.65590e-6
$q_2(\theta_3)_{\mu,p}$	0.303916	3.98738e-4	-9.15743e-6

Table 3: Parameters of the energy dependence of parameters p_i for the flux model of proton-originated secondaries. From top to bottom: e.m. particles from proton showers; muons from proton showers. The four $\theta_0 \div \theta_3$ values are the centers of four bins in the $[0° \div 65°]$ polar angle range where primaries have been generated with Corsika, as discussed *supra*.

In the expressions above we have denoted with $P(N|\lambda)$ the Poisson probability of observing in a detector N secondary particles of each species from a shower whose mean number of particles inside the detector area at the detector location is λ, and with $G(T - t^{\exp})$ the probability of observing a time difference $T - t^{\exp}$ of the signal with respect to that expected from the shower development; above, G is a Gaussian distribution with expected value of 0 and variance σ_T^2. The λ and $t^{\exp}$ values are a function of the already described model, and of the hypothesis for the primary particle identity.

4.4   Likelihood Maximization

Once the set of data $N_{e,i}, N_{\mu,i}, T_{e,i}, T_{\mu,i}$ is specified, the logarithm of the expression given in Equation 13 is a function of the hypothesis on the identity of the primary particle, and of five parameters that fully determine the shower model: the intersection of the shower axis on the ground X_0, Y_0 (dubbed 'shower core'); the polar and azimuthal angles θ_0, ϕ_0, *i. e.* the shower direction; and the primary energy E_0. The maximization of the log-likelihood can be performed numerically once derivatives with respect to each of the five parameters are estimated.

The model detailed in Sec. 3 describes particle densities as a function of the distance of the detecting unit location $(x_i, y_i, 0)$ (where we have chosen the elevation z to be 0 at the detector plane) from the shower axis. When the polar angle θ is non-null, this distance can be computed by expressing the coordinates of points on the shower axis as a function of a parameter ξ, and finding the value of ξ^* corresponding to the closest point to the unit by setting to zero the derivative of the expression of the distance with respect to ξ:

$$x = X_0 + \xi \sin\theta \cos\phi \qquad y = Y_0 + \xi \sin\theta \sin\phi \qquad z = \xi \cos\theta \tag{15}$$
$$d = ((x_i - x)^2 + (y_i - y)^2 + z^2)^{0.5} \tag{16}$$
$$\xi^* = (x_i - X_0)\cos\phi\sin\theta + (y_i - Y_0)\sin\theta\sin\phi \tag{17}$$

The distance of detector i from the shower can then be computed as:

$$R_i = \sqrt{(x_i - X_0)^2 + (y_i - Y_0)^2 - \xi^{*2}} \tag{18}$$

We may now express the derivative of the log-likelihood function over shower parameters X_0, Y_0, θ, ϕ as follows:

$$\frac{d\ln\mathcal{L}}{dX_0} = \sum_i \left[\frac{d\ln\mathcal{L}}{dR_i}\frac{dR_i}{dX_0} + \frac{d\ln\mathcal{L}}{dt_i}\frac{dt_i}{dX_0} \right], \qquad \frac{d\ln\mathcal{L}}{dY_0} = \sum_i \left[\frac{d\ln\mathcal{L}}{dR_i}\frac{dR_i}{dY_0} + \frac{d\ln\mathcal{L}}{dt_i}\frac{dt_i}{dY_0} \right], \tag{19}$$

$$\frac{d\ln\mathcal{L}}{d\theta} = \sum_i \left[\frac{d\ln\mathcal{L}}{dR_i}\frac{dR_i}{d\theta} + \frac{d\ln\mathcal{L}}{dt_i}\frac{dt_i}{d\theta} \right], \qquad \frac{d\ln\mathcal{L}}{d\phi} = \sum_i \left[\frac{d\ln\mathcal{L}}{dR_i}\frac{dR_i}{d\phi} + \frac{d\ln\mathcal{L}}{dt_i}\frac{dt_i}{d\phi} \right], \tag{20}$$

with

$$\frac{dR_i}{dX_0} = \frac{-(x_i - X_0) + \xi^*\sin\theta\cos\phi}{R_i}, \qquad \frac{dR_i}{dY_0} = \frac{-(y_i - Y_0) + \xi^*\sin\theta\sin\phi}{R_i}. \tag{21}$$

$$\frac{dt_i}{dX_0} = -\sin\theta\cos\phi/c, \qquad \frac{dt_i}{dY_0} = -\sin\theta\sin\phi/c \tag{22}$$

$$\frac{dR_i}{d\theta} = -\xi\cos\theta\left[(x_i - X_0)\cos\phi + (y_i - Y_0)\sin\phi\right]/R_i, \qquad \frac{dR_i}{d\phi} = -\xi\sin\theta\left[-(x_i - X_0)\sin\phi + (y_i - Y_0)\cos\phi\right]/R_i \tag{23}$$

$$\frac{dt_i}{d\theta} = \cos\theta\left[(x_i - X_0)\cos\phi + (y_i - Y_0)\sin\phi\right]/c, \qquad \frac{dt_i}{d\phi} = \sin\theta\left[-(x_i - X_0)\sin\phi + (y_i - Y_0)\cos\phi\right]/c \tag{24}$$

$$\tag{25}$$

where the latter two expressions are derived by assuming that the shower front moves at the speed of light c.

To complete the calculations we also need explicit derivatives of the log-likelihood function by E_0, which directly depends on the shower model, and by detector distances and expected arrival times R_i and T_i; these are computed as follows:

$$\frac{d\ln\mathcal{L}}{dE_0} = \sum_i \left[\frac{d\ln\mathcal{L}}{d\lambda_{e,i}}\frac{d\lambda_{e,i}}{dE_0} + \frac{d\ln\mathcal{L}}{d\lambda_{\mu,i}}\frac{d\lambda_{\mu,i}}{dE_0} \right], \qquad \frac{d\ln\mathcal{L}}{dR_i} = \frac{d\ln\mathcal{L}}{d\lambda_{e,i}}\frac{d\lambda_{e,i}}{dR_i} + \frac{d\ln\mathcal{L}}{d\lambda_{\mu,i}}\frac{d\lambda_{\mu,i}}{dR_i} \tag{26}$$

$$\frac{d\ln\mathcal{L}}{dt_{e,i}^{\exp}} = \frac{T_{e,i} - t_{e,i}^{\exp}}{\sigma_T^2}, \qquad \frac{d\ln\mathcal{L}}{dt_{\mu,i}^{\exp}} = \frac{T_{\mu,i} - t_{\mu,i}^{\exp}}{\sigma_T^2}. \tag{27}$$

Finally, the derivatives of the log-likelihood function by the flux expectations $\lambda_{e,i}$, $\lambda_{\mu,i}$ at detector i are simply

$$\frac{d\ln\mathcal{L}}{d\lambda_{e,i}} = -1 + \frac{N_{e,i}}{\lambda_{e,i}}, \qquad \frac{d\ln\mathcal{L}}{d\lambda_{\mu,i}} = -1 + \frac{N_{\mu,i}}{\lambda_{\mu,i}}. \tag{28}$$

Derivatives of expected fluxes λ by distance from detector R_i, shower energy E_0, and polar angle θ have been already discussed in Sec. 4.2. The maximization of $-\ln\mathcal{L}$ is performed with the ADAM optimization scheme [13]. An explicit expression of all the derivatives has been given above because it is used in the code to obtain derivatives of the likelihood ratio test statistic described below (Sec. 4.5).

4.5 The Likelihood Ratio Discriminator

The biggest challenge of a ground-based gamma observatory is to successfully distinguish the almost purely electromagnetic showers of secondaries that these primary rays originate from the mixed electromagnetic-hadronic showers generated by primary hadrons (protons or light nuclei, hereafter only addressed by as proton showers) as shown in Fig. 1. The ratio between the flux of primary gammas and hadrons is already much smaller than 1 for GeV-energy showers, and it rapidly falls to values below 10^{-4} for the PeV-energy showers whose rate and origin constitute one of the main scientific goals of a high-energy gamma-ray observatory.

There are multiple discriminating features which can be exploited to distinguish gamma primaries from protons; by far the most striking one is the number and distribution of the hard component, composed of energetic muons produced by pion and kaon decays in the atmosphere. Leveraging the simplistic model of secondaries density on the ground we have developed in Sec. 4.2, we will concern ourselves only with the radial distribution of these particles in the following.

The classification problem can be cast as one of hypothesis testing, when Neyman-Pearson's (NP) lemma ensures that the most powerful test statistic to distinguish two simple hypotheses is a log-likelihood ratio. Although we are in this case not under the conditions of validity of the NP lemma, given that the hypotheses under test are composite (the log-likelihood values depend on the five parameters defining a shower under each primary hypothesis), the log-likelihood ratio still retains good properties, once we evaluate it for the value of parameters that maximize the two likelihoods: this is thus a profile likelihood ratio,

$$\mathcal{T} = \ln\frac{\mathcal{L}_\gamma(\hat{X}_0, \hat{Y}_0, \hat{\theta}, \hat{\phi}, \hat{E}_0)}{\mathcal{L}_p(\hat{X}_0, \hat{Y}_0, \hat{\theta}, \hat{\phi}, \hat{E}_0)} = \ln(\mathcal{L}_\gamma^{\max}) - \ln(\mathcal{L}_p^{\max}). \tag{29}$$

Please note that in the above expression, the estimators $\hat{X}_0, \hat{Y}_0, \hat{\theta}, \hat{\phi}, \hat{E}_0$ at the numerator are different from those at the denominator, as each of them refers to a different primary hypothesis (gamma at the numerator, proton at the denominator). We consider the above test statistic as the source of our discrimination of gamma showers from proton backgrounds in the rest of this work. Each factor in $\mathcal{T}$ is obtained by the likelihood maximization procedure described above. We can use the likelihood ratio as our primary tool to extract inference on the flux of gamma primaries from a set of detected showers, and that inference will be used to compute a utility function that tracks the sensitivity of the experiment to the gamma spectrum at different energies. The optimization loop searching for the most advantageous configuration of detectors on the ground will then require us to obtain derivatives of that utility function with respect to the detectors position, x_i, y_i. We provide those calculations in Sec. 6.

4.6 Performance of Shower Reconstruction

As secondary densities decrease sharply both as a function of the distance of a detection unit from the shower axis, and as a function of the energy of the primary, the minimization of the above $-\ln\mathcal{L}$ function is highly non trivial, and special care must be taken to prevent the algorithm from getting stuck in local minima. In particular, the correct identification of the shower axis (parameters X_0, Y_0) is problematic when the shower center is far from the detector array and only few detector units have been hit by secondaries.

In order to ease the identification of the absolute minimum of $-\ln\mathcal{L}$ we perform an initialization of the parameters by computing the value of $-\ln\mathcal{L}$ in a grid of points, in two steps. We start with angular parameters θ_0, ϕ_0, whose value is mostly sensitive to the timing information and is relatively decoupled from that of the other three parameters. We use a grid of 4 by 4 values of (θ_0, ϕ_0) in $[0° \div 65°] \times [0 \div \pi]$, and set $(X_0, Y_0) = (0\,\mathrm{m}, 0\,\mathrm{m})$ and $E_0 = 1\,\mathrm{PeV}$ as values for the shower core and energy; the grid values of θ_0 and ϕ_0 corresponding to the largest of the 16 likelihoods are used as initialization values for the following step. The initialization procedure for the X_0, Y_0 and E_0 coordinates is CPU-heavy, as we need to scan three dimensions and these parameters are strongly correlated. For the typical runs of the algorithm discussed below we use a grid of 1000 values (10 by 10 values of X_0, Y_0 and 10 values of energy).

Once initialized parameters are set, a full maximization of the likelihood is performed by gradient descent using the ADAM optimizer. The precision with which shower parameters are correctly measured by the maximization procedure also depends on the size of the detector array. While the procedure described above could certainly be improved in a real offline analysis of individual detected showers, the added precision would only be very loosely coupled with the signs of gradients on the utility function, and would thus not affect significantly the question on the table, namely the exact location of detector units; hence by sticking to a well-defined reconstruction procedure, even if potentially sub-optimal and CPU-limited, we may still reasonably hope that the result will track the reality of the detector performance.

4.7 Triggering

A parameter which has the potential of affecting the optimal layout of detection units is the minimum number of tanks which record a signal (of muons or e.m. particles) in events that we accept in our selection. If that number is too small, the inference on the origin of the shower or on the shower parameters is insufficiently precise to make a difference, so it makes sense to filter those events out. We set the threshold for accepting showers in the calculation of the gamma flux and the utility to $N \geq 10$ detection units. If we do that, we need to also inform the gradients of the utility function of the probability that a shower falls off acceptance if we move a detector from its current position.

For the purpose of updating gradients correctly, we compute the probability that a detector observes at least one secondary particle of any kind (muons or e.m. particles) by evaluating:

$$S(N_{\mathrm{obs}} \geq 1) = \sum_{i=1}^{N_{\mathrm{det}}} \left(1 - \exp(-\hat{N}_{\mu,i} - \hat{N}_{e,i})\right) \tag{30}$$

as the sum of probabilities over detector units to detect at least one particle of any kind, where $\hat{N}_{\mu,i}$, $\hat{N}_{e,i}$ are expected fluxes at each detector, and use it to derive:

$$p(N_{\mathrm{active}} \geq N_{\mathrm{trigger}}) = 1 - \sum_{k=0}^{N_{\mathrm{trigger}}-1} [\mathrm{Poisson}(k, S)] \tag{31}$$

In other words, we approximate the combinatorial probability that out of a total of N_{det} detectors at least N_{trigger} of them have seen a signal, by using the approximated combined probability of small p-values as their sum. The approximation above works quite fine for our purposes, and it has been shown to approximate to better than $2\,\%$ the true probability in practical situations of relevance to this study, which are restricted to cases when the number of detectors giving a signal is not too different from the threshold N_{trigger}.

The above formulas can be easily differentiated with respect to the position of detectors x_i, y_i by using the chain rule and by observing that changes of detector positions affect the expected fluxes $\hat{N}_{\mu,i}$, $\hat{N}_{e,i}$. So, $e.\,g.$, to obtain the derivative of the probability that a shower passes the trigger condition with respect to a dx_{i^*} movement of detector i^*, we compute

$$\frac{dp}{dx_{i^*}} = -\frac{d}{dx_{i^*}} \left[\sum_{j=0}^{N_{\text{trigger}}-1} \left(\mathrm{e}^{-S} S^j / j! \right) \right]. \tag{32}$$

By recalling the definition of S, now making explicit the expected fluxes into detector i^*,

$$S = \sum_{i=1}^{N_{\text{det}}} \left[1 - \mathrm{e}^{(-\lambda_{\mu,i} - \lambda_{e,i})} \right] \tag{33}$$

we get

$$\frac{dP_{\text{active}}}{dx_{i^*}} = -\sum_{j=0}^{N_{\text{trigger}}-1} \left[\frac{1}{j!} \left(\mathrm{e}^{-S} (S^j - j S^{j-1}) \right) \frac{dS}{dx_{i^*}} \right] \tag{34}$$

5 Extraction of the Signal Fraction Uncertainty from Batches of Showers

A measurement of the flux of gamma rays entails the reconstruction of the showers observed in a given time interval, as well as the estimate of the fraction of observed showers genuinely due to gamma primaries. As described above, we rely on a likelihood ratio test statistic to separate gamma from proton primaries. Once we simulate a batch of gamma and proton cosmic rays corresponding to the wanted integration time, we reconstruct them under the two hypotheses, and proceed to compute the test statistic value for each shower. Rather than using the test statistic to select a gamma-rich subset, however, we directly fit for the fraction of gamma primaries in the batch by a likelihood maximization. This allows to avoid the non-differentiable operation of selecting test statistic values above a hard-set cut.

In a batch of N_{batch} showers, for each of which we have a measured value of $\mathcal{T}$, we can estimate the fraction of photons f_γ by maximizing the likelihood:

$$\mathcal{L}(f_\gamma) = \prod_{i=1}^{N_{\text{batch}}} \left[f_\gamma P_\gamma(\mathcal{T}_i) + (1 - f_\gamma) P_p(\mathcal{T}_i) \right], \tag{35}$$

where with $P_\gamma(\mathcal{T}_i)$ $(P_p(\mathcal{T}_i))$ we have expressed the probability density function of the test statistic for gamma (proton) showers.

5.1 Construction of the PDFs of the Test Statistic

We construct a model of the density function of the test statistic $\mathcal{T}_\gamma$ ($\mathcal{T}_p$) by substituting a Gaussian kernel to each value of $\mathcal{T}$ for a set of gamma (respectively, proton) showers. The sigma of the Gaussian kernel needs to be a fair estimate of the true uncertainty of the value of $\mathcal{T}$, which depends on the varying conditions under which different showers are measured. The procedure is the following:

1. We simulate N_{events} showers, half of which are from gamma primaries and half from proton primaries. Shower parameters are sampled such that their centers cover the area instrumented by detectors with a wide enough margin that showers falling beyond the area do not produce a meaningful signal in the array. As for angular and energy parameters, the polar angle is sampled from a $dN/d\cos(\theta)^2$ distribution; primary energy is sampled from a falling power law distribution in the $[0.1\,\mathrm{PeV}, 10\,\mathrm{PeV}]$ range.

2. We proceed to reconstruct them under both primary hypotheses using the likelihood maximization described in Sec. 4 above. obtaining a test statistic value from each from the log-likelihood difference $\mathcal{T}(i) = \ln\left(\mathcal{L}_{\mathrm{max}}^\gamma\right) - \ln\left(\mathcal{L}_{\mathrm{max}}^{\mathrm{proton}}\right)$;

3. We compute the uncertainty on the value of $\mathcal{T}$ for each shower k by considering the Poisson variations of the observed number of electrons/gammas and muons in each detector, and the Gaussian variations of their arrival times:

$$
\sigma_{\mathcal{T}_k}^2 = \sum_{i=1}^{N_{\mathrm{det}}} \left[\left(\frac{d\mathcal{T}_k}{dN_{\mu,i}}\right)^2 N_{\mu.i} + \left(\frac{d\mathcal{T}_k}{dN_{e,i}}\right)^2 N_{e,i} + \left(\frac{d\mathcal{T}_k}{dt_{\mu,i}}\right)^2 \sigma_{t_{\mu,i}}^2 + \left(\frac{d\mathcal{T}_k}{dt_{e,i}}\right)^2 \sigma_{t_{e,i}}^2 \right] \tag{36}
$$

4. We model the PDF of gamma and proton test statistics by summing Gaussian distributions, each centered at the observed value of $\mathcal{T}_k$ of the set of $N_{\mathrm{events}}/2$ gammas and protons, and renormalizing the resulting distributions to unit integral:

$$
P(\mathcal{T}_\gamma) = \frac{2}{N_{\mathrm{events}}} \sum_{k=1}^{N_{\mathrm{events}}} I_k(\gamma) G(\mathcal{T}_k, \sigma(T_k)) \tag{37}
$$

$$
P(\mathcal{T}_p) = \frac{2}{N_{\mathrm{events}}} \sum_{k=1}^{N_{\mathrm{events}}} I_k(p) G(\mathcal{T}_k, \sigma(\mathcal{T}_k)) \tag{38}
$$

where the indicator function I_k is 1 (0) if the primary particle is of the requested kind.

5.2 Estimate of the Variance

In order to construct a meaningful utility function to optimize, we do not need an estimate of f_γ, but rather an estimate of its uncertainty given the experimental conditions under which it has been extracted.

To be precise, we would be most interested in the mean squared error of the gamma fraction, including in our consideration a possible bias in the fraction estimate. A bias in the estimate may arise from the measurement process as well as from the raw data, produced by the actual geometry

of the detector array; we consider that the bias can be corrected for *a posteriori*, so we concentrate on the variance only. The variance of f_γ can be estimated by using Rao-Cramer-Frechet's bound:

$$\sigma_{f_\gamma}^2 = \left[-\frac{d^2 \ln \mathcal{L}}{df_\gamma^2} \right]^{-1}. \tag{39}$$

The second derivative of the log-likelihood function can be obtained as:

$$-\frac{d^2 \ln \mathcal{L}}{df_\gamma^2} = \sum_i \left[\frac{[P_\gamma(\mathcal{T}_i) - P_p(\mathcal{T}_i)]^2}{[f_\gamma P_\gamma(\mathcal{T}_i) + (1 - f_\gamma)P_p(\mathcal{T}_i)]^2} \right] \tag{40}$$

and from this we obtain an estimate of the variance on f_γ, using Equation 39.

5.3   Selection of Showers

While it makes little sense to apply selection cuts to the showers in the approach we have taken, which aims to extract all the available information on the photon flux from the full distribution of the likelihood ratio test statistic, we would still like to inject some realism in the data collection procedure, by only considering showers that are detected simultaneously by a minimum number of detector elements. As already mentioned above (Sec. 4), we consider a threshold of 10 units recording at least one particle (either muon or electron/photon) and select within each batch only those shower passing this criterion in all calculations.

The problem with setting such a threshold is that the number of detectors observing a signal is a quantity for which we cannot produce derivatives. This prevents the correct evaluation of the gradient of the utility with respect to detector displacements on the ground, as getting one detector farther from a shower may indeed affect that quantity – it may result in that shower to fall below threshold, and to thus not be included in the set that is used for the calculation of the Utility.

We solve the problem by considering expectation values of the secondary particle fluxes in each detector, and by approximating the probability that the triggering threshold is passed by a shower. The calculation goes as follows.

We recall how we defined the probability that unit i observes at least one ($N_{\text{obs}} \geq 1$) particle from shower j as

$$P(N_{\text{obs}} \geq 1)_{ij} = 1 - \exp(-\lambda_\mu(x_i, y_i) - \lambda_e(x_i, y_i)) \tag{41}$$

where we have now used the expectation values of the fluxes of secondaries at the position of detector i. The probability that shower j causes at least N_{trigger} detectors to see a signal is then computable by considering all combinations of detectors, but with 6000 units or more this calculation is too CPU expensive. We resort to the following approximation: we construct the sum

$$P_{\text{tot}}(j) = \sum_{i=1}^{N_{\text{det}}} P(N_{\text{obs}} \geq 1)_{ij} \tag{42}$$

and with it define the probability that the shower has at least N_{trigger} detectors observing secondaries as

$$P_{\text{tr}}(j) = 1 - \sum_{k=0}^{N_{\text{trigger}}-1} \text{Poisson}(k|P_{\text{tot}}(j)) \tag{43}$$

The above constitutes an approximation, which we need to check. We therefore simulate showers in various detectors configurations, resample the number of secondaries observed in each detector unit to obtain an expectation value of the probability for each shower to pass the $N > N_{\text{trigger}}$ requirement, and compare it to the result of the calculation above. We find a good agreement between the two numbers in all tested configurations. Figure 9 shows one typical comparison, which exhibits good linearity and sufficient precision for our task.
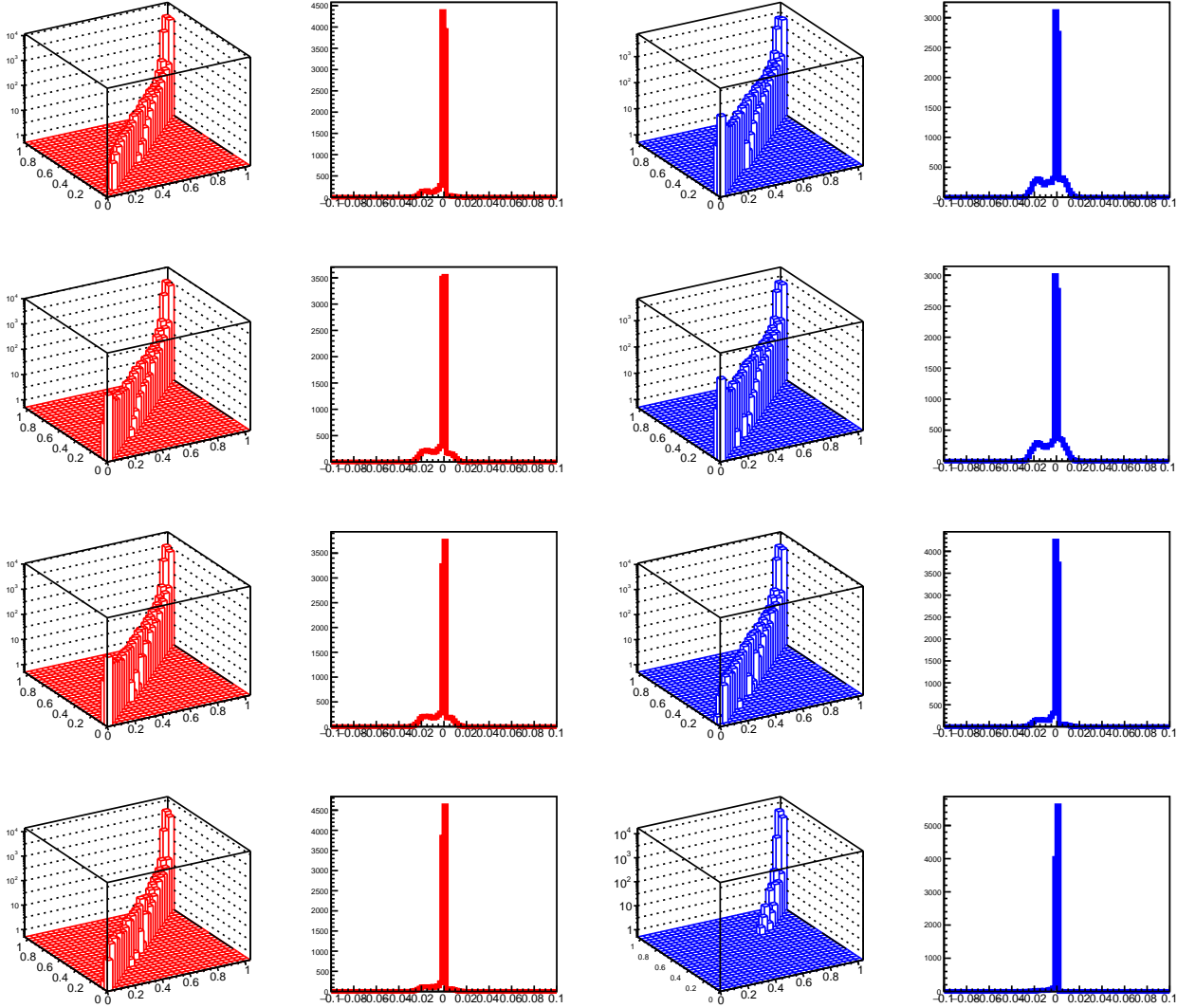

Figure 9: Probability to yield signal in 10 detector units for gamma (red) and proton (blue) originated showers of four different energies (from top to bottom 0.2,0.5,1.4,2.9 PeV for gammas, and correspondingly 0.1, 0.2, 0.5, 1 PeV for protons), for a test configuration of the detector elements. The probability is computed by repeated sampling (axis toward right in 3D graphs) as well as by the approximated formulas described in the text (axis toward left). The right panel of each pair shows the difference between the two calculations, which is seen to lie within 0.03.

The formulas above are easily differentiable so we may incorporate them in the calculations of gradients. In particular, they affect the calculation of the probability that a shower belonging to a batch is included in the likelihood formulas used to extract the flux and its uncertainty, and their

derivatives.

Finally, we note that the probability that a shower leaves a signal in a sufficient number of detector units is a function of energy and distance from the array. In order to ensure that we fully test the functionality of arrays, we need to carefully choose the area illuminated by showers in the detector plane, such that we extend it past the sensitive area. Shower generation and reconstruction is a CPU-costly factor in the optimization loop, so the two criteria are conflicting –a wider illuminated area tests more carefully the array performance, but it also spreads a fixed number of generated showers per epoch to smaller density, which is detrimental for the precision of the inference; or, if the density is kept fixed, it requires a larger number of showers per batch. In Fig. 10 we show the probability that a shower leaves a signal in at least 10 detector units (each unit comprising seven standard tanks of $R = 1.9\,\mathrm{m}$ in a packed hexagonal set) for the two cases of primary identity (gamma or proton) as a function of the distance of the shower core on the ground from the closest detector, and as a function of the energy of the primary particle in PeV. To create the figure, we considered an array only consisting in 61 units in a tight hexagonal arrangements, such that the array extension on the ground was small enough to give a sound meaning to the studied distance from the core; of course, a more numerous array would have a larger probability to globally fulfil the $N > 10$ criterion, but the observed cutoff in the distance distribution would not move very significantly if the triggering condition were correspondingly raised. We observe that a good compromise between illumination and density/CPU constraints is to generate showers at no less than 2000 meters from the closest detector.
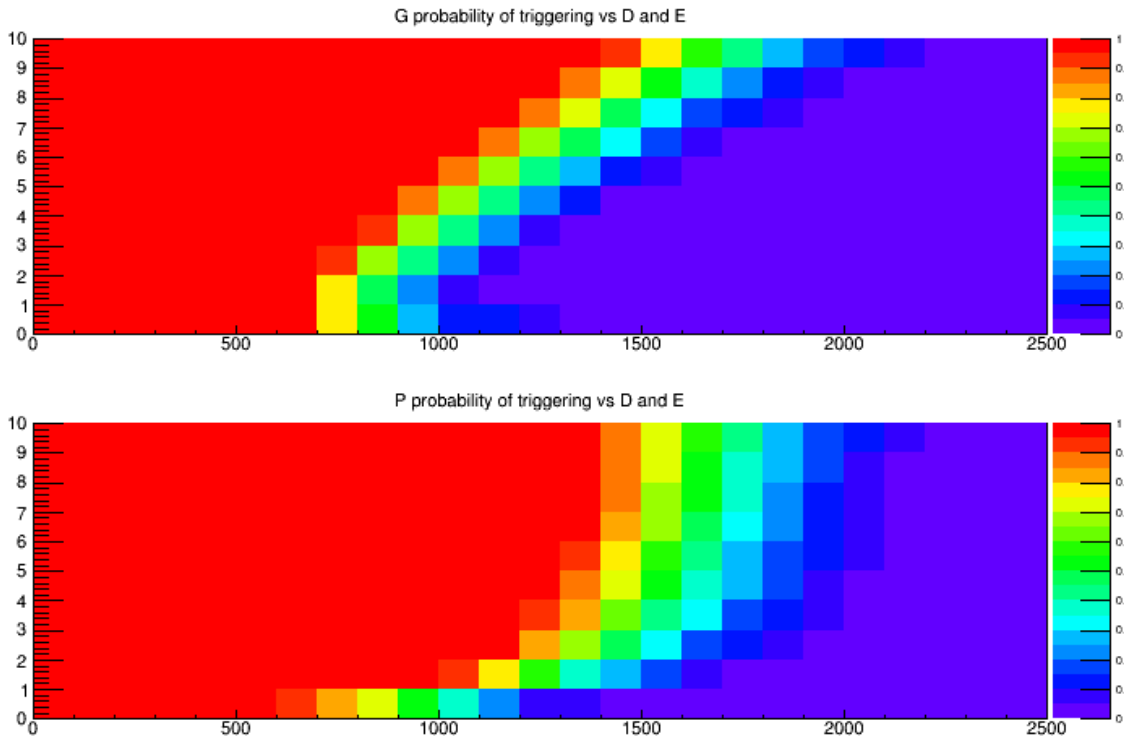

Figure 10: Triggering probability for primaries of different energy (vertical axis, in PeV) and distance from the closest detector of a circular array (horizontal axis, in meters). Top: photon primaries; bottom: proton primaries. See the text for more detail.

26

5.4 Derivative of P_{tr}

The calculation of the derivative of the utility function with respect to movements of the detectors on the ground, which we describe below (Sec. 6), requires as a factor the derivative of the above-calculated triggering probability P_{tr} with respect to the position x_i, y_i of each detector ($i = 1...N_{\text{det}}$). The calculation is straightforward. We have:

$$\frac{dP_{\text{tr}}(m)}{dx_i} = -\frac{d}{dx_i} \sum_{k=0}^{N_{\text{tr}}-1} \left[e^{-S(m)} \frac{S(m)^k}{k!} \right] \quad \text{with} \quad S(m) = \sum_{i=1}^{N_{\text{det}}} \left[1 - e^{[-\lambda_{\mu,i}(m) - \lambda_{e,i}(m)]} \right]. \tag{44}$$

The latter function can be differentiated by $e.\,g.\,\,dx_i$, obtaining

$$\frac{dS(m)}{dx_i} = -\frac{d}{dx_i} \left[e^{[-\lambda_{\mu,i}(m) - \lambda_{e,i}(m)]} \right] e^{[-\lambda_{\mu,i}(m) - \lambda_{e,i}(m))]} \left(\frac{d\lambda_{\mu,i}}{dx_i} + \frac{d\lambda_{e,i}}{dx_i} \right). \tag{45}$$

Using the above expression, from Equation 44 one then finally obtains the derivative of $P_{\text{tr}}(m)$ over x_i. The calculation of the derivatives of fluxes λ with respect to the detector position has already been discussed *supra*.

6 Calculation of the Utility Function and its Derivatives

We are now ready to consider an expression for the global utility which might trace the overall scientific goals of the considered experiment. It would be myopic and arrogant to try and encode into a single number the vast range of measurements and searches that could be planned for such an instrument. However, the goals of this document is to show how such a number, if one can agree upon its definition, may successfully guide the design of the array; we have no presumption that the choice of a utility made in this document has any merit *per se*. With that in mind, we can discuss a possible choice, which is a crucial ingredient of the optimization pipeline we aim to test.

6.1 Two-component Utility Definition

We believe that a considerable scientific interest in astroparticle physics today is offered by the very high-energy gamma showers that can be measured at energies of a PeV and above –a region that has generated interest after LHAASO published the observation of a small but significant number of candidates [14]. In general, the measurement of the gamma flux in the 100 TeV to 10 PeV region can be taken as a good initial bid for the main goal of a large ground-based Cherenkov array in this document. We therefore define the following utility function:

$$U_1 = \frac{\Phi_\gamma}{\sigma_{\Phi_\gamma} \sqrt{\rho}}, \tag{46}$$

where the density factor ρ at the denominator is discussed below. The function above is an integrated measure of the precision in the determination of the gamma flux Φ_γ in the $0.1\,\text{PeV} \div 10\,\text{PeV}$ range. Such a function could be subdivided into pieces that described the relative value of a precise flux measurement in smaller energy intervals. Such a fine-tuning has been neglected at present, and it may be the subject of a future extension, pending a discussion within the collaboration of the relative value that should be assigned to precision versus energy. We however notice how the choice of the coefficient in the power law governing the energy distribution of the generated showers effectively

plays the same role of a weighting factor: a large negative value of the power corresponds to giving all the importance to the low-energy end of the sample, and a large positive value instead privileges the contribution of high-energy showers. For most of our studies we kept the energy distribution of generated showers flat, in order to explicitly avoid any bias of that kind in the generated solutions.

While the scaling of the flux uncertainty at the denominator of U_1 with $1/\sqrt{N_{\text{batch}}}$ is a reasonable assumption, it would be better to avoid it altogether, and to generate at every epoch during optimization a sufficiently large flux of showers in a fixed region surrounding the array, wide enough to allow detector units to move around without seeing a decreased flux. We plan for longer runs of the pipeline that may accommodate this safer mode of operation in the future; results presented in this document are instead making use of the above assumed scaling. The utility definition thus contains a factor $1/\sqrt{\rho}$, where the density is computed per batch. At each epoch, the area where we generate showers is determined by the following procedure:

1. The average radial extension $\overline{R}$ of the array is evaluated;

2. a constant R_{slack} ($2\,\text{km}$ by default[3]; see Sec. 4.7) is added to $\overline{R}$;

3. showers are generated at a random position (with constant density in x, y) within a circle of radius $R_{\text{tot}} = \overline{R} + R_{\text{slack}}$ from the origin of the axes on the detector plane;

4. showers that are found to be at a distance exceeding R_{slack} from any of the array detectors are discarded and substituted with newly generated ones; the number of total generated trials N_{trials} is stored.

5. the procedure stops when N_{batch} shower positions are obtained; energy, polar and azimuthal angle of incidence, and identity of each shower are assigned at random.

At the end of the above procedure, which is repeated at every epoch during optimization, the area uniformly covered by the N_{batch} showers is computed as:

$$A = \pi R_{\text{tot}}^2 \frac{N_{\text{batch}}}{N_{\text{trials}}}. \tag{47}$$

The density of showers per unit area on the ground in a batch then scales (omitting the π term) with:

$$\rho \propto \frac{N_{\text{trials}}}{R_{\text{tot}}^2}. \tag{48}$$

A second ingredient in a global utility function should be the precision of the estimate of relevant parameters of gamma-originated showers: energy, as well polar and azimuthal angle of incidence of the primary particle in the atmosphere. On the contrary, the two parameters describing the core position on the ground (X_0, Y_0) should be considered nuisance parameters in the estimation problem: they contain no physics information on the primary flux. As the precision on angular parameters mostly depends on the timing measurement of the detector units, we for the time being neglect to consider in the utility, and concentrate on specifying a gauge of the resolution on the energy. A suitable function of energy resolution is the following:

---

[3]The use of the average of the radial extension of the array causes, in later stages of an optimization run, units that have drifted to high radius to "see" a smaller than $2\,\text{km}$ radius of generated showers around them. This is acceptable for the exploratory runs we made, and can also be considered an implicit limit in the radial extension we want to consider. The need for using the average array radius and not the radius of the outermost unit is to avoid issues with the differentiability of the utility.

$$U_2 = \frac{\sum_{k=1}^{N_{\text{batch}}} P_{\text{tr}}(k) W(k) \frac{E_{t,k}^2}{\delta^2 E_{t,k}^2 + (E_{t,k} - E_{m,k})^2}}{\sum_{k=1}^{N_{\text{batch}}} P_{\text{tr}}(k) W(k)}. \tag{49}$$

Above, the δ^2 parameter has been set to 0.1, which is close to the scale of the relative resolution of the energy of gamma showers obtained in many of the considered configurations. Its presence at the denominator of the U_2 function above has the purpose of regularizing its value, avoiding a too large contribution to the utility from showers whose energy is by chance reconstructed to be equal to the true one. U_2 is thus a growing function of the precision in the energy reconstruction, which plateaus when shower energies are all measured with a relative precision well below 30 %. A weighting factor $W(k)$ is further introduced to give more importance to the precise energy reconstruction of higher-energy showers. In this model, the weight $W(k)$ has the following form:

$$W(k) = 1 + \ln(E(k)/E_{\text{min}}) \tag{50}$$

with $E_{\text{min}} = 0.1\,\text{PeV}$, the lower range of the considered shower energies.

The two factors U_1 and U_2 can be used in alternative, or combined in a multi-objective utility once suitable multipliers assessing their relative value are chosen. We have experimented with different combinations, but for our preliminary investigations –whose purpose is mainly to verify the functioning of the software– and the results detailed in this work we have used the following definition:

$$U = \eta_{f_\gamma} U_1 + \eta_{\Delta E} U_2 \tag{51}$$

A choice of $\eta_{f_\gamma} = 0.1$ and $\eta_{\Delta E} = 10.$ provides in many of the performed tests a rough balancing of the two components of the utility. This choice is totally arbitrary at this point, but it has the merit of allowing us to study the interplay of the two components in the optimization loops.

While the U_2 factor is independent on the number of showers that is generated on the ground at each epoch, and is only dependent on the maximum distance from detector units that is illuminated by the generated flux of primaries (the larger this distance, the worse the reconstruction of showers becomes), the U_1 factor strongly depends on the density of generated showers per unit area. Since we need to compare results that employ different number of showers per batch, and configurations that have arbitrary areas covered with detectors, a correction is necessary. To a first approximation, a correction factor consists in multiplying, as we have already done in Equation 46 above, the flux-dependent term by $1/\sqrt{\rho}$, where ρ is the number of generated showers per batch per unit square kilometer. The factor compensates for the variance of the flux estimate, as the latter scales with the Poisson mean.

6.2 Derivatives of the Utility

The calculation of the derivatives of the utility function is a CPU-heavy task, given the need of iterating, for every detector, on the batch of showers generated at each epoch, tracking the value of partial derivatives that inform the utility about the effect of a movement in x or y of a tank. We detail below the essential ingredients of the calculation.

6.2.1 Derivatives of U_1 term

The expression of U_1 contains an estimate of the flux of photons, given a certain integration time, and an estimate of the uncertainty on the flux estimate. As discussed in Sec. 5, both quantities are

obtained from the derivatives of the log-likelihood function as a function of the fraction of gamma-originated showers, given the set of observed values of test statistic in a batch of showers.

To compute the derivative with respect to the x_i position of detector i along one coordinate, we need to compute:

$$\frac{dU_1}{dx_i} = U_1 \left(\frac{1}{f_\gamma} \frac{df_\gamma}{dx_i} - \frac{1}{\sigma_{f_\gamma}} \frac{d\sigma_{f_\gamma}}{dx_i} - \frac{0.5}{\rho} \frac{d\rho}{dx_i} \right) \tag{52}$$
$$= U_1 \left[\frac{1}{f_\gamma} \frac{df_\gamma}{dx_i} - \frac{1}{\sigma_{f_\gamma}} \frac{d\sigma_{f_\gamma}}{dx_i} + \frac{1}{R_{\text{tot}}} \frac{dR_{\text{tot}}}{dx_i} - \frac{0.5}{N_{\text{trials}}} \frac{dN_{\text{trials}}}{dx_i} \right]$$

Let us consider each derivative in the expression above in turn.

The estimate f_γ is the result of setting to zero the derivative of the two-component likelihood function. We may compute its derivative with respect to x_i by implicit differentiation. We treat f_γ as the dependent variable and the probabilities $p_\gamma(k)$, $p_p(k)$ as independent variables, and use the chain rule to relate the derivation by p_γ and p_p to derivation by x_i. Let us first define

$$H = \frac{d\ln\mathcal{L}}{df_\gamma} = \sum_k \left[\frac{p_\gamma(k) - p_p(k)}{f_\gamma p_\gamma(k) + (1 - f_\gamma)p_p(k)} \right] = 0 \tag{53}$$

as the equation that defines f_γ. We now differentiate with respect to x_i, obtaining:

$$\sum_k \left[\frac{dH}{dp_\gamma(k)} \frac{dp_\gamma(k)}{dx_i} + \frac{dH}{dp_p(k)} \frac{dp_p(k)}{dx_i} \right] + \frac{dH}{df_\gamma} \frac{df_\gamma}{dx_i} = 0 \tag{54}$$

whence

$$\frac{df_\gamma}{dx_i} = -\frac{1}{\frac{dH}{df_\gamma}} \sum_k \left[\frac{dH}{dp_\gamma(k)} \frac{dp_\gamma(k)}{dx_i} + \frac{dH}{dp_p(k)} \frac{dp_p(k)}{dx_i} \right]. \tag{55}$$

Now we have:

$$\frac{dH}{df_\gamma} = -\sum_m \left[\frac{(p_\gamma(m) - p_p(m))^2}{(f_\gamma p_\gamma(m) + (1 - f_\gamma)p_p(m))^2} \right] \tag{56}$$

(Note that the last expression is minus the inverse of the estimated variance on f_γ). If we further define, for brevity:

$$\Delta(m) = p_\gamma(m) - p_p(m), \qquad D(m) = f_\gamma p_\gamma(m) + (1 - f_\gamma)p_p(m), \tag{57}$$

we can write:

$$\frac{dH}{dp_\gamma(k)} = \frac{[D(k) - \Delta(k)f_\gamma]}{D(k)^2} = \frac{p_p(k)}{D(k)^2} \tag{58}$$

and

$$\frac{dH}{dp_p(k)} = \frac{-[D(k) + \Delta(k)(1 - f_\gamma)]}{D(k)^2} = -\frac{p_\gamma(k)}{D(k)^2}. \tag{59}$$

Finally, we obtain

$$\frac{df_\gamma}{dx_i} = \frac{\left[p_p(k) \frac{dp_\gamma(k)}{dx_i} - p_\gamma(k) \frac{dp_p(k)}{dx_i} \right]}{D(k)^2 \sum_m \left(\frac{\Delta(m)^2}{D(m)^2} \right)}. \tag{60}$$

As far as the x_i derivatives of the probabilities of the observed test statistic under the two hypotheses are concerned, they are obtained by considering that the latter are obtained from sums of Gaussian terms, *e. g.*,

$$p(\mathcal{T}_\gamma)(k) = \sum_{m=1}^{N_{\text{ev}}} \left[P_{\text{tr}}(m) \frac{\exp[-\frac{(\mathcal{T}(m)-\mathcal{T}(k))^2}{2\sigma_T^2(m)}]}{(2\pi\sigma_{\mathcal{T}}^2(m))^{0.5}} \right]. \tag{61}$$

We can differentiate over dx_i directly, obtaining

$$\frac{dp_\gamma(k)}{dx_i} = \sum_m \left[P_{\text{tr}}(m)G(m,k) \left(\frac{\mathcal{T}(m)-T(k)}{\sigma_{\mathcal{T}}^2(m)} \left(\frac{d\mathcal{T}(k)}{dx_i} - \frac{d\mathcal{T}(m)}{dx_i} \right) \right. \right. \tag{62}$$

$$+ \frac{[\mathcal{T}(m)-\mathcal{T}(k)]^2}{2\sigma_{\mathcal{T}}^4(m)} \frac{d\sigma_{\mathcal{T}}^2(m)}{dx_i} - \frac{1}{(2\pi\sigma_{\mathcal{T}}^2(m))^{1.5}} \frac{d\sigma_{\mathcal{T}}^2(m)}{dx_i} + \frac{1}{P_{\text{tr}}(m)} \frac{dP_{\text{tr}}(m)}{dx_i} \right) \Bigg] \tag{63}$$

where we have used the concise expression $G(m,k) = \frac{\exp[-\frac{(\mathcal{T}(m)-\mathcal{T}(k))^2}{2\sigma_T^2(m)}]}{(2\pi\sigma_{\mathcal{T}}^2(m))^{0.5}}$. Similar expressions to those above are found for derivatives versus y_i and for derivatives of $p_p(k)$.

Finally, we need to consider the contributions to dU_1/dx_i of the derivatives of R_{tot} and N_{trials} factors. As far as the former is concerned we have simply

$$\frac{dR_{\text{tot}}}{dx_i} = \frac{1}{N_{\text{batch}}} \frac{x_i}{R_i} \tag{64}$$

where R_i is the distance of detector i from the origin of axes. For N_{trials}, which is not differentiable, we need instead to resort to an approximate calculation. We consider the distance R_{it}, $t = 1...N_{\text{trials}}$ of each shower core generated in the trial procedure from detector i, and then:

1. if the trial failed to be included in the set of N_{batch} showers, we compute varied distances from shower t $R'_{it,\Delta x}$, $R'_{it,\Delta y}$ corresponding to detector i moves by arbitrary increments Δx, Δy in turn (setting them to the typical movement of detectors at each epoch); if the shower meets the $R < R_{\text{slack}}$ criterion after the move, counters ΔN_x, ΔN_y are correspondingly increased;

2. if the trial shower is part of the batch, we test if its distance from detector i is the only one below the threshold R_{slack}; in that case, we determine if a movement Δx or Δy would cause the criterion to fail, and if so we decrement counters ΔN_x and/or ΔN_y accordingly.

At the end of the procedure, the needed derivatives of N_{trials} are simply found as

$$\left(\frac{dN_{\text{trials}}}{dx_i}, \frac{dN_{\text{trials}}}{dy_i} \right) = \left(\frac{\Delta N_x}{\Delta x}, \frac{\Delta N_y}{\Delta y} \right). \tag{65}$$

6.2.2 Derivatives of U_2 term

The second part of the utility function defined *supra*, U_2, contains an explicit dependence on the measured energy of showers. The derivative of the term by the displacements dx_i, dy_i is then straightforward to obtain. Here we only show the result for dx_i:

$$\frac{dU_2}{dx_i} = \frac{N'D - ND'}{D^2} \tag{66}$$

with

$$N = \sum_k \left[P_{\text{tr}}(k)W(k)\frac{E_t(k)^2}{\delta^2 E_t(k)^2 + (E_t(k) - E_m(k))^2} \right]$$

$$D = \sum_k P_{\text{tr}}(k)W(k)$$

$$N' = \sum_k \left[\frac{dP_{\text{tr}}(k)}{dx_i}W(k)\frac{E_t(k)^2}{\delta^2 E_t(k)^2 + (E_t(k) - E_m(k))^2} \right.$$
$$\left. + \frac{2P_{\text{tr}}(k)W(k)E_t(k)^2(E_t(k) - E_m(k))}{[\delta^2 E_t(k)^2 + (E_t(k) - E_m(k))^2]^2}\frac{dE_m(k)}{dR_{ik}}\frac{dR_{ik}}{dx_i} \right]$$

$$D' = \sum_k \frac{dP_{\text{tr}}(k)}{dx_i}W(k). \tag{67}$$

6.3 Verification of the Derivatives with `derivgrind`

Forming the derivative by hand, as we do above, is tedious and error-prone. For many pieces of our derivative computation code, we have verified their correctness by comparing their results to derivatives computed with algorithmic differentiation (AD). AD is a set of techniques to evaluate derivatives of computer code with floating-point accuracy. Specifically, we use the forward mode of AD with a single AD input x, which is based on the idea to keep track of a "dot value" $\dot{a} = \frac{\partial a}{\partial x}$ for every real number a handled by the computer code to be differentiated. Any global variables have an initial dot value of 0, and the AD input x – i.e., the variable with respect to which we want to obtain algorithmic derivatives – receives a dot value of $\frac{\partial x}{\partial x} = 1$. Now, whenever a new real number is computed in the code to be differentiated, typically by elementary floating-point arithmetic operations (e.g. $c = a \cdot b$), its dot value can be computed according to the appropriate differentiation rule (e.g. $\dot{c} = \dot{a} \cdot b + a \cdot \dot{b}$). For any AD output – i.e., any variable that we want to differentiate with respect to the single AD input x –, the derivative $\frac{\partial y}{\partial x}$ can then be read from $\dot{y}$.

AD tools implement this procedure by analyzing computer code for real- arithmetic operations, and inserting such "AD logic", in a semi- automatic fashion. Many AD tools operate directly on the source code (e.g. `Tapenade`), use language features like operator overloading (e.g. `CoDiPack`, `JAX`, and the internal tools of `PyTorch` and `TensorFlow`), or hook into a compiler that builds the code to be differentiated (e.g. `Enzyme, Clad`). `derivgrind` [15] is a novel AD tool that operates on the machine code of the compiled program. This is advantageous for us as it minimizes the amount of modifications to the source code necessary in order to apply the AD tool – to compute a derivative $\frac{\partial y}{\partial x}$, we merely needed to identify x and y in our C++ source code, and apply macros `DG_SET_DOTVALUE` and `DG_GET_DOTVALUE` from a header `derivgrind.h`, respectively.

Parts of the optimization code is organized in subroutines that take a specific argument `mode`, evaluate a function if `mode` is 0, and derivatives of the function with respect to relevant variables if `mode` is larger than zero. For these routines, the calculation with `derivgrind` is straightforward, as shown in Fig. 11.

`derivgrind` can handle multi-threading and third-party libraries like ROOT out of the box. While `derivgrind` does not run as fast as source-code-based AD tools targeted to high performance setups, this is not a concern for us as the derivative checks do not run in production.

In all of our checks, the analytic derivatives match `derivgrind`'s algorithmic derivatives. This indicates that we correctly derived and implemented the analytic derivatives.

```cpp
#include <valgrind/derivgrind.h>

double f(double x1, double x2, int mode) {
  if(mode==0){
    // ... return f(x1,x2) ...
  } else if(mode==1) {
    // ... return df(x1,x2)/dx1
  } else if(mode==2) {
    // ... return df(x1,x2)/dx2
  }
}

int main(){
  // ... initializations ...
  double x1=3.1, x2=42.0; // some test values

  double one = 1.0;
  DG_SET_DOTVALUE( &x1, &one, sizeof(double) );
  // evaluate f, could also have multiple statements here
  double result = f(x1,x2,0);
  double df_dx1_algorithmic = 0;
  DG_GET_DOTVALUE( &result, &df_dx1_algorithmic, sizeof(double) );
  std::cout << "ALGORITHMIC DERIVATIVE: " << df_dx1_algorithmic <<
std::endl;

  double df_dx1_analytic = f(x1,x2,1);
  std::cout << "ANALYTIC DERIVATIVE: " << df_dx1_analytic << std::endl;
}
```

Figure 11: *Evaluation of the algorithmic derivative* $d\!f/d\!x1$ *of a function f with Derivgrind. The user can then compare it with the analytic derivative.*

7 The End-to-end Optimization Loop

The optimization loop runs on the pipeline described in blocks in [Sec. 3](). Besides initializations of the optimization run parameters, definition of the starting layout of the detector array, and of the shower model, the loop aims at computing the utility of the current configuration and the derivatives of the utility with respect to x and y movements of each of the detector units in turn; the latter are used to update the detector positions, when the loop can be repeated.

The computing-heavy parts of the above cycle are two: a first cycle on the requested gamma and proton showers, which are generated and reconstructed by likelihood maximization under the two hypotheses in turn; and a cycle on detector units, when derivatives of the utility are computed. These two cycles are decoupled from the rest of the computation, and performed by multithreading, when each of the N_{CPU} available CPUs is tasked with reconstructing N_{events}/N_{CPU} showers in the first, and computing derivatives for N_{det}/N_{CPU} of the units. This arrangement speeds up the overall speed of the program by a factor that approaches N_{CPU}, if N_{events} and N_{det} are both integer multiples of N_{CPU}.

The code is available in both a standalone C++ version and as a ROOT macro. Running under ROOT allows to monitor the histograms showing current configuration, utility, and a wealth of other metrics, and is useful for debugging purposes; no multithreading has been implemented in the ROOT macro version at the moment.

7.1 Initialization and Run Parameters

A starting configuration for the array must be specified during the initialization of the program. This involves deciding a value of these parameters:

1. the number of tanks comprising the array, N_{det};

2. the location of each tank on the ground, x_i, y_i;

3. the size of each tank, assumed circular, R_{tank}; all tanks are assumed to be of the same size in the runs we performed so far, but a specification of different geometries for each tank is straightforward.

The optimization loop requires the user to specify a number of other details. We provide here a list to give a view to the functionality and options that are currently implemented in the code:

- the number of showers generated at each epoch for the calculation of the PDF of the test statistic of proton and photon showers, N_{events};

- the number of showers generated at each epoch to test the performance of the array, N_{batch};

- the number of epochs for the optimization;

- the starting epoch. This is useful in case an optimization run is performed on a configuration that has already been worked at previously, so that all the program outputs retain the same numbering;

- whether the detector positions are to be read from an input file;

- the shape of the generated array. There are several options available, from a circular uniformly filled array, to sets of detectors placed in a circle at fixed radius, to two or three such sets, or to a set of random values within a square.

- the starting learning rate for detector movements;

- the coefficient of the utility related to the flux precision, η_{GF};

- the coefficient of the utility related to the energy resolution part, η_{IR};

- the minimum number of units that have to see at least one secondary particle, N_{trigger}, in order for the shower reconstruction to be performed;

- the slope of the power law determining the energy distribution of generated showers.

Additional options include the turning off of reconstruction of specific parameters for showers (*e. g.*, angles, core position, or energy), the option of generating showers orthogonal to the ground, and the number of grid points scanned in the initialization of shower parameters for their reconstruction.

One additional parameter called CommonMode must be discussed separately. This is used to decide whether detector positions are updated independently at each iteration of the gradient descent loop (CommonMode=0),

$$x_i \to x_i' = x_i + \eta(i)\frac{dU}{dx_i} \tag{68}$$

$$y_i \to y_i' = y_i + \eta(i)\frac{dU}{dy_i} \tag{69}$$

(where $\eta(i)$ is the total learning rate of unit i, see *infra*), or whether instead a common movement is computed for classes of detectors that share the same radius (CommonMode=1), or the same symmetrical position around the origin, in a multiplicity decided by the user through the value of CommonMode. For example, if CommonMode is set to three, the initial layout of the detector units is set up such that triplets of detectors are set at the same radius and at azimuthal positions around the origin offset by 0, 120, and -120 degrees, such that they form the pattern of an equilateral triangle. After individual gradients are computed, the new position of each element of the triplet is determined by computing the average radial displacement of the three units, and the average azimuthal rotation. The three units positions are then updated according to those averages. The procedure reduces the stochasticity of the utility derivatives, and at the same time ensures that the overall layout of the detector retains an overall symmetry according to the multiplicity specified by the parameter. Since this strategy has proven very effective, most of the results shown in this document are produced with CommonMode=3, 4, or 6.

7.2   Learning Rate Scheduling

In order to facilitate the convergence to a meaningful configuration corresponding to a stable maximum of the utility, a learning rate must be specified and carefully adapted to the evolving task. Each unit (or set of units, if the optimization is run with CommonMode equal to 3 or larger) needs to move by an amount that is on average smaller than the distance of the unit to its neighbors: this makes more effective the procedure of independently moving each unit in series, as it minimizes the correlations of the effect of movements of neighboring units.

Another condition that the learning rate must fulfil is to slowly decrease, to let the system slowly drift to an optimal configuration. This trend may be enriched by including oscillatory increases and decreases, as such a schedule often helps the search in complex multi-dimensional spaces. We have experimented with a few different options and finally settled on an exponential decrease of the learning rate, which gets damped by a factor of $\exp(\alpha_0)$ from the start to the end of the optimization, while oscillating with a squared cosine shape:

$$\eta_c = \exp(-\alpha_0 x/N_{\text{epochs}}) \left[\alpha_1 + (1 - \alpha_1) \cos^2(\alpha_2 x/N_{\text{epochs}})\right] \tag{70}$$

where x is the epoch, ranging from 0 to N_{epochs}. Suitable values for $\alpha_{0,1,2}$ are $e.\,g.$ $(2, 0.8, 20)$, whereby the damping over the full cycle amounts to a factor of $\exp(2)$ with about six oscillations. The above factor is a common learning rate, and it applies to all units. On top of that, it is useful to track the individual movements of the units, and correct the learning rate of each unit differently, increasing the mobility of units that consistently move in some direction and damping the mobility of units that oscillate around some particular position. To achieve that goal, the position of each unit is recorded during gradient descent, and the following quantity is evaluated at each epoch:

$$\cos\theta_{\text{eff},i} = \frac{(x_i^n - x_i^{n-1})(x_i^{n-1} - x_i^{n-2}) + (y_i^n - y_i^{n-1})(y_i^{n-1} - y_i^{n-2})}{\left[(x_i^n - x_i^{n-1})^2 + (y_i^n - y_i^{n-1})^2\right]^{0.5} \left[(x_i^{n-1} - x_i^{n-2})^2 + (y_i^{n-1} - y_i^{n-2})^2\right]^{0.5}} \tag{71}$$

The factor above is used together with the global scheduling in determining the overall multiplier of each unit's utility gradient:

$$\eta(i) = \eta_c \exp(k \cos\theta_{\text{eff},i}) \tag{72}$$

with k set to producing a small correction per epoch, $k = 0.05$; the build up of the correction may however have a significant effect over several epochs (typically, a damping one). Finally, the displacement of each unit in x and y is capped at a maximum allowed value, to prevent abnormally high gradients from disrupting the smooth learning of configurations. This maximum value is usually set at half the initial detector spacing.

7.3 Other Detail

A number of other details need to be specified in order to produce a working model of reconstruction, inference, and meaningful utility gradients. We list here some of them.

- In the optimization procedure we are implicitly assuming that stochastic gradient descent will allow the progressive drift of an initial layout to a more advantageous configuration. This is reasonable inasmuch as it is akin to the independent update of each of the weights and biases of a neural network layer. Detector positions are modified in series, one by one, without a guarantee that the combination of the movements produces an overall improvement in the utility, but convergence should be guaranteed in the long run. The local guarantee of a utility increase would only exist for infinitesimal displacements, but the large CPU demand of the task mandates that the learning rate multiplier of each unit's utility gradients be finite and not too small. We have observed that indeed the learning rates are a critical parameter in the success of an optimization run. Trial and error here is the only way to approach the issue.

- While tanks (or macro-tank aggregates, such as those we employ in our initial investigations) have a physical size (a $R = 1.9$ m radius), their movement on the ground is left unconstrained by the presence of nearby tanks: it may thus happen, as it does relatively frequently, that two tanks end up being displaced to an almost coincident location –a configuration which would be impossible to realize in practice. We are undeterred by this feature, however, as an iterative correction of overlapping tank positions can easily be implemented at the end of an optimization run (the procedure would be to start with the closest pair of tanks, moving them away from their mutual center until they are separated by the desired amount $R_{\min}$, and to iterate until no pair is closer than $R_{\min}$). Such a correction, given the scale of the typical investigated areas with respect to the tank dimensions, would affect the utility in a negligible way.

8   Results

In this section we present some preliminary results obtained with the algorithm discussed in the previous sections. Due to the large CPU demand of the optimization loop, we have not yet been able to study systematically the full problem of the layout of O(6000) detector units; such a task should be only performed after a thorough beta testing of the code, and once the program has been modified to include a detailed modeling of tank efficiencies and response versus angle, number of particles, and energies. The purpose of the results we show here is instead only demonstrative: we wish to show how the optimization pipeline is capable of identifying non trivial solutions that maximize the given utility, and how such solutions share common features that, *a posteriori*, make physical sense. We have thus constrained so far to considering "macro-tank" aggregates of 19 units of 1.9 m radius, tightly packed in a hexagonal setup (See Fig. 12).

8.1   Size of the Array

The first thing that becomes apparent, once an optimization run is performed starting with a layout consisting of detectors uniformly spread in a confined region, is that gradients of the utility –in particular, the U_1 part in Equation 46– point outwards. In other words, the layout wants to expand to a larger area, in order to catch more gamma showers that are otherwise hard to reconstruct and discriminate from proton backgrounds. This phenomenon exists even if the $\rho^{-0.5}$ factor in U_1 is omitted: a larger flux of secondaries from showers produced at 1 km or more from the center of the array allows for a larger likelihood ratio of the gamma versus proton hypothesis of those showers, which ends up improving the precision of the flux estimate when a two-component fit to the test statistic is carried out. The presence of the density factor further enhances the advantage of a radial expansion, as in hindsight should be easy to understand: a flux measurement will benefit from a larger sensitive area.

In contrast with the above phenomenon, the U_2 term in the utility does not produce large outward-pushing gradients. Similarly to the flux uncertainty, a better energy resolution is also warranted by a more intense flux of secondaries, but the U_2 factor integrates energy resolutions in a wide range, and although we have inserted in it an energy-dependent weight that privileges the correct estimate of very high-energy showers, the effect is less clear and also less easy to understand intuitively. It is precisely this kind of interplay between conflicting criteria that makes the appraisal of layouts a task unfit for back-of-the-envelope calculations. It is also to be noted that the coefficient of the power spectrum of the generated gamma showers plays a very important role in determining both the size and the behavior of the U_2 term. For this reason, we have set the power to zero in our studies,
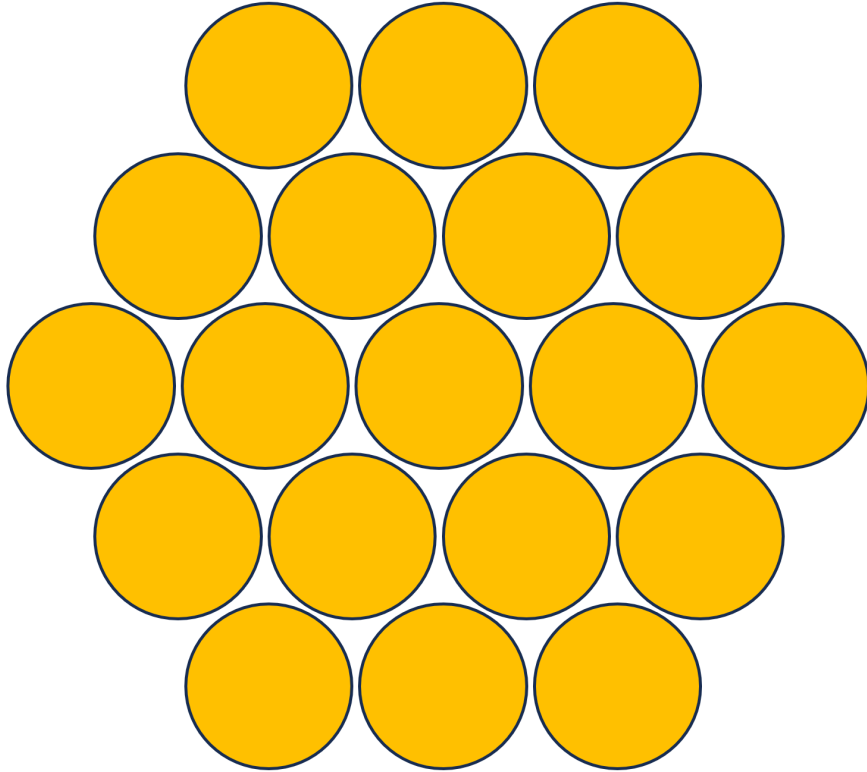
Figure 12: Layout of 19 tanks used as a macro-unit to reduce computations

pending a discussion on the utility specification.

8.2   Radial Distribution of Tanks

The other effect which can be observed almost immediately in optimization loops that start with a uniformly populated area on the ground (whatever its shape) is that, in conjunction with an expansion of the array, the program finds no rationale in populating the center of any symmetrical configuration. While keeping a radially symmetric distribution, the utility gradients cause a shear of the center of the array, moving toward larger radii the units initially placed at the center faster than those at the edges. This is a separate phenomenon from the one discussed *supra*, although it originates from the same physical reason, namely the existence of a dimensional scale in the problem (the transverse size of photon-originated showers).

Why should a hole-in-the-middle donut-like configuration be providing a smaller flux uncertainty than a flat disc distribution of units? The answer is simple: the center of the array is a point of measure zero –odds that a shower has its core in that place are null. Even the task of measuring low-energy gammas is not better attended by a densely populated distribution of units, as there is a quadratically larger number of showers hitting larger radii than there are at smaller radii. For that reason, a donut is to be preferred to a disc, and this appears a conclusion without appeal. Only if one had infinite integration time and were concerned solely with the energy resolution of the few showers one could collect in a small patch of ground, would the strategy of putting all the units in the "same basket" work. Any other experimental condition will instead prefer a more distributed layout which "looks toward the boundary", and tries to catch as much information as possible from

the R^2-growing flux of showers.

8.3 Effects of Reconstruction Requirements

Since a precise reconstruction of the five shower parameters increases the discriminating power of the likelihood ratio, and consequently reduces the uncertainty on the signal fraction in a batch, we may expect that optimal configurations be strongly dependent on how well the reconstruction can be carried out. A way to observe this phenomenon, with a view to gaining more understanding on the way optimal configurations are selected by the algorithm, is to check how the reduction of the complexity of the reconstruction task modifies the optimal layouts. Or, from the opposite standpoint, we may start with a simpler reconstruction task and progressively make it more complex, if we start by assuming that we know some of the shower parameters.

We may, *e. g.*, assume that angular and energy parameters are perfectly known, and only task the algorithm with measuring the shower cores. A further simplification is to assume that all showers have zero polar angle, *i. e.* that they come down orthogonally, leaving circular footprints. In this case, we observe that the system loses any interest in populating the ground with a two-dimensionally distributed array, and produces optimal configurations in the shape of thin annuli, or triangular shapes if a triangle degeneracy is enforced. The reason for this behavior is rather easily understood: once the energy of the shower is given, the flux is a simple function of the distance of the core, so that no "stereo" information is needed to disentangle the effect of energy and distance on the intensity of the flux.

When angular parameters are also unknown, and showers are generated with the standard distribution of polar angles, the reconstruction problem becomes slightly more complex; timing information allows to determine the azimuthal direction of the shower and its tilt from the vertical only if some two-dimensional information on the actual shower footprint is collected by the array. We then observe that more distributed configurations are preferred.

The integrated energy resolution term in the utility function plays a role if the energy of the showers is not assumed known. The optimal configurations can then be observed to distribute tanks on the ground in richer two-dimensional shapes, dictated by the need to acquire more information on the distance of the core together with the overall intensity. Of course, a modification of the relative value of the coefficients in the two terms of the utility function will significantly affect the optimal configurations.

Finally, we may experiment with the reconstruction performance by letting all five parameters be identified as usual by the likelihood maximization, but easing the task with an initialization of the parameters to their true values. This guarantees that the likelihood will quickly find the absolute maximum and the best estimates. In fact, this *modus operandi* should probably be our default, as in real life we may expect to have all the CPU time we need to solve the reconstruction task in the best possible way for every shower. What we observe if we run the program this way is that convergence speeds up significantly, and stochasticity in the utility evaluation gets massively reduced; the configurations found by the program are however similar to those found by the standard mode of running.

In summary, we observe that some of the detailed characteristics of the reconstruction problem as it is posed have a strong impact in the outcome of the optimization task; others less so. The utility specification is however crucial. Rather than discouraging us from searching for the best configuration, this consideration and the richness of the problem should motivate us to study it further. We discuss further *infra* the different behavior of optimal configurations when different utility specifications are imposed.

8.4 Effects of the Triggering Condition

The requirement that a minimum number of units has observed at least one secondary particle is a detail we decided to include in the model because it has a clear impact in the optimization task. In fact, ground configurations that disperse the tanks too much may impact the number of reconstructable showers, as the active units become likely to fall below the triggering threshold. The condition we studied, $N \geq N_{\text{trigger}} = 10$, is rather mild and is easily passed by sufficiently energetic showers when the array is compact, especially when we consider a total number of units of the order of 6000. However, when we study the behavior of the algorithm with a smaller total number of units, the threshold imposes a constraint on how much can units get spaced away from one another. We indeed observe that if we *e. g.* optimize a small array made of 37 macro-tanks (corresponding to 703 units), the utility gets maximized by splitting the array into two parts, with units in each remaining close by, and moving farther apart to "conquer" more ground and consequently increasing their capability of observing a large number of high-energy showers (see Fig.13). Each of the two parts is then made up of a bit less than 20 units, which collectively have a significant chance of detecting more than 10 particle signals.
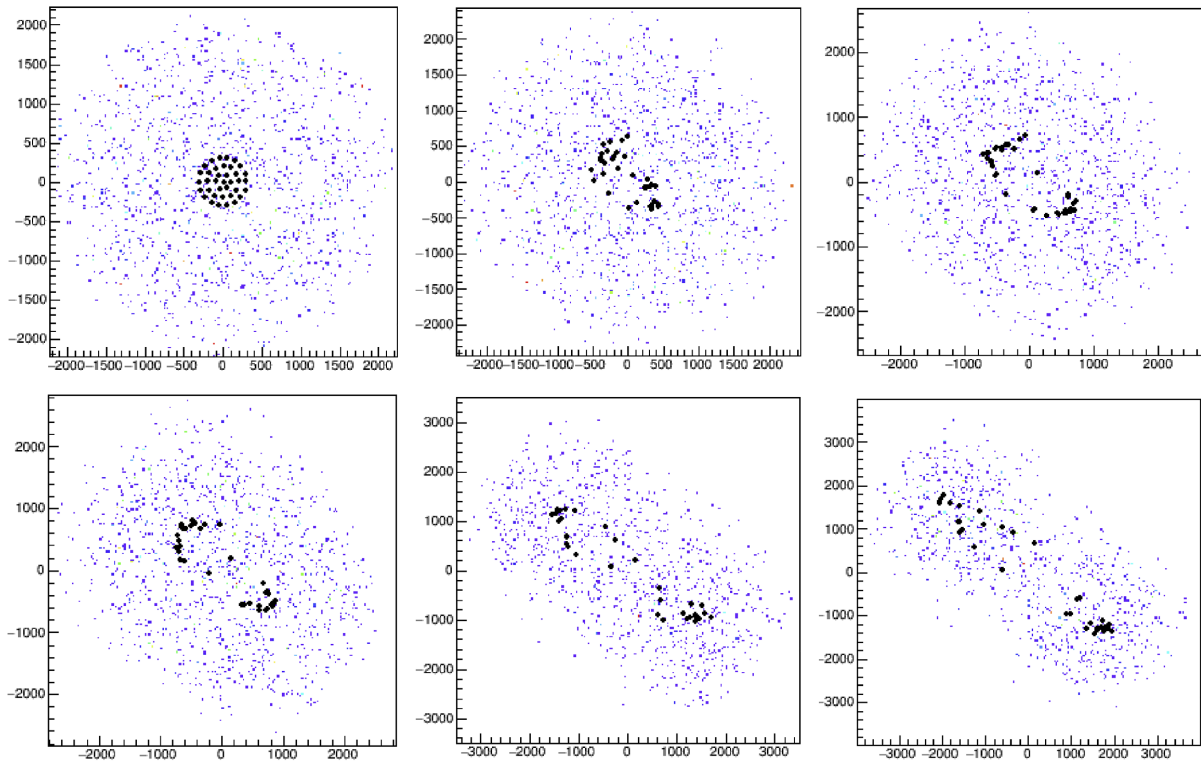

Figure 13: Effect of the $N_{\text{trigger}} \geq 10$ condition on the optimization of a small array of 37 elements. The array (black points) is shown at different epochs, starting from epoch 2 (top left) to epoch 200 (bottom right). Also shown are the positions of showers that are accepted by the trigger selection. Note how the horizontal and vertical scales widen as detectors move apart, while retaining a feature of two islands roughly splitting the total number of units in two.

The above mentioned effect remains an important ingredient even when the system is constituted by hundreds of units, and we believe (although we have not run extensive optimizations in those conditions) even when it comprises several thousands. The reason is that there will always be an

advantage in keeping a number of tanks (or macro-tanks, when we simplify the computing task by aggregating units in groups) close together, if their number guarantees that the group is independently capable of recording showers falling at arbitrary distances from their common center. What the system evolves to, in these circumstances, are configurations that spread multiple sets of units in rather exotic configurations.

The above observations constitute one further demonstration that the layout optimization problem we posed is way more complex than one would naively consider it to be, when the problem is specified with the necessary level of detail (concerning, as we have seen until here, the reconstruction task, the triggering condition, and the complexity of the utility function). Further complications will no doubt arise when the response of individual tanks will be characterised in detail for its efficiency, capability of counting precisely or less so the number of secondaries and their energy, and so forth.

8.5   Symmetries

When triplets of units are locked together in an equilateral shape, it is reasonable to expect that the optimization will converge to configurations where a triangular symmetry is apparent; this is not a rule, as the array has complete freedom in arranging itself into non-trivial configurations within a 120-degree sector; rather, its emergence after a few dozen loops of gradient descent updating signals that coherent gradients are winning over stochastic noise.

The program allows one to experiment with a higher number of units locked together into squares, pentagons, hexagons, or even full radial symmetry (this option is available when CommonMode is set to 1), when all units placed at the same initial radius will only move radially in synchrony. We however believe that the triangular symmetry configurations reached by runs with CommonMode=3 are the most instructive ones to study: the evolution from an initial uniform arrangement to shapes such as those of Fig. 15 during gradient descent contains information on the stability of the intermediate solutions and hints at ways to explore more fully the configuration space.

The convergence to symmetrical configurations of varied complexity –and sometimes eerie abstraction, as Fig. 15 demonstrates– does not imply that the optimization task is completed. On the contrary, it in fact proves that the task of finding the *best* configuration in a landscape of similarly good-performing ones is a quite difficult one: the utility landscape is, in other words, riddled with a large number of local maxima. A more aggressive scheduling of the learning rate may be needed to break that impasse. However, it lays beyond the intended purpose of the present version of this document, which is rather more a description of the algorithm than its final exploitation to find the best configuration. In fact, that final step will be most proficuous when the shortcuts and approximations we have taken will have been sorted out.

8.6   Results with U_1 Alone

For a proof of the convergence of different initial layouts to similar final configurations, we simplified the optimization task by only considering the U_1 part of the utility function, and by generating showers orthogonally to the ground. We further reduced CPU consumption by assuming that the energy of the showers be measured precisely, only tasking the reconstruction algorithm with estimating the shower core positions. We employed initial layouts of 126 tanks [4] arranged in a tightly-packed ball (with spacing of 50 m between units), a random distribution of units in a twice wider circle, and a two-annuli configuration. We set CommonMode to 3, so that each of the 42 triplets of units can

---

[4]For the two-annuli configuration the number is 129 because of the need to distribute units in an equally spaced manner in the two rings.
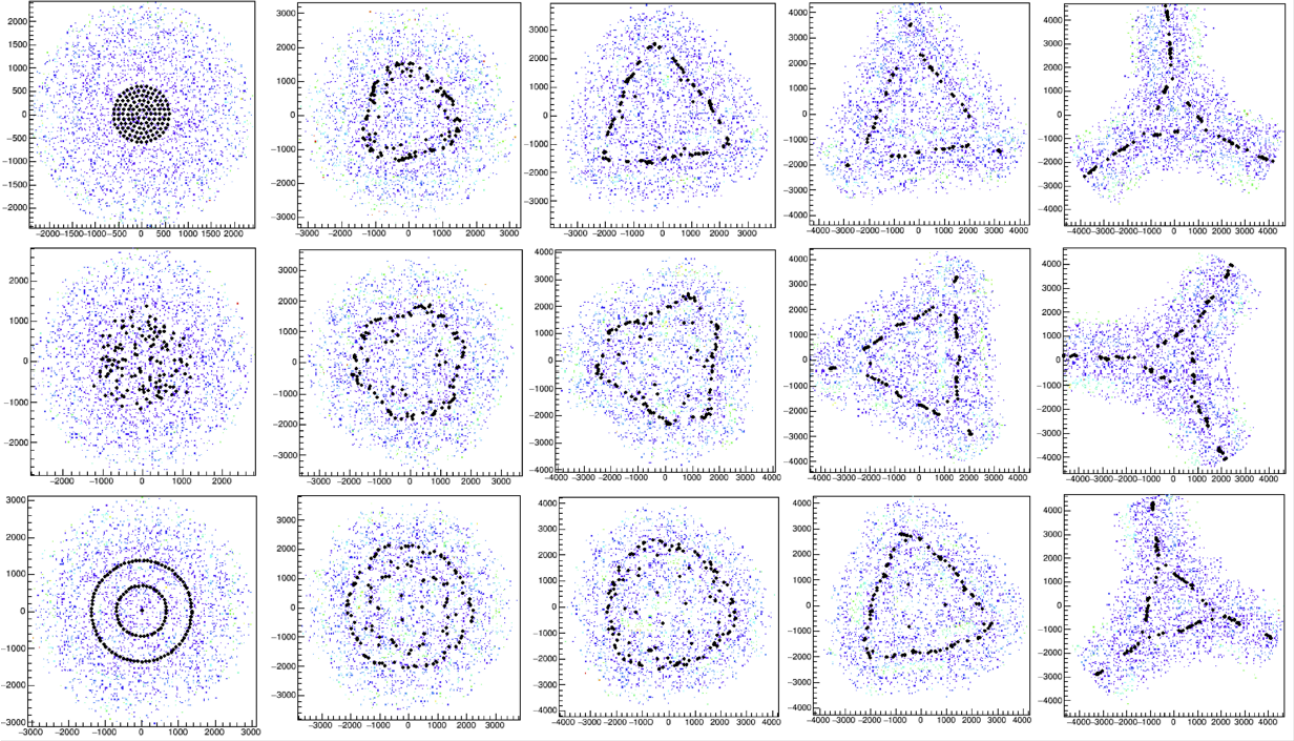
Figure 14: Convergence of three initial layouts (top to bottom: packed ball, wide random ball, two annuli) during a 500-epochs training. From left to right, the configurations of 126 units (129 in the bottom one) are shown at epoch 1,50,150,300, 500. See the text for more detail.

move freely but respecting the triangular symmetry of their initial configuration. Using 2000 events for the PDF estimation and 2000 batch at every epoch, each job takes about 4 days of running for 500 epochs on a single core.

The results are summarized in Fig. 14, where the three initial configurations are shown on the left, and they are seen evolving to triangle-symmetric configurations as the 42 triplets of units move coherently in search of the maximum utility. Despite the initial difference in the layouts, the final ones are virtually equal to one another, confirming that the system brought them to converge to a stable maximum of the utility. The values of the utility of the three final configurations also converge to similar values, as shown in Table 4 below.

Configuration	Units	$U_1(0)$	$U_1(500)$
Tightly packed ball	126	109.6	138.2
Wide random ball	126	124.6	135.7
Two annuli	129	135.8	140.1

Table 4: Values of the utility at the start of the optimization cycle (epoch 0) and at the end (epoch 500) for the three configurations described in the text. Since these layouts include 126/129 macro-tanks composed of 19 standard A1 tanks, their utility should be compared to standard layouts composed of 126*19 (129*19) = 2194 (2451) units.

42

8.7 A Result Using the Full Expression of U

Given the work-in-progress nature of this document, we do not yet have a final answer on what could be the most effective layout of O(6000) detector units once we include all terms in the utility and remove some of the simplifying assumptions with which we have *e.g.* demonstrated *supra* the correct convergence of the algorithm to the same configurations starting from different initial setups. Part of the reason for this temporary lack of finalized results is the high CPU demand of full-fledged optimization cycles, as we observed that 2000 epochs or more may be needed to convergence in the most general case (when all five parameters of showers are simultaneously fit, and showers are generated with a distribution of polar and azimuthal angles). In those conditions, even if sticking to 300 macro-units, an optimization loop running on 30 CPU in parallel will require of the order of two weeks to complete.

What we can show for the time being is the result of an optimization run which still assumes orthogonal showers (polar angle zero), but which includes the task of reconstructing the energy of showers along with their core positions. In Fig. 15 we show the behavior of the utility, as well as a few configurations reached by the program during gradient descent, and the final result. We draw the attention to the reader to the utility values at the start of the optimization (for a tightly packed ball, with units spaced by 50 m) and the utility reached after 1760 epochs, which are equal[5] to

$$U_{ep=0\div3} = U_1(0\div3) + U_2(0\div3) = 140.0 + 41.7 = 181.7 \pm 10.8$$
$$U_{ep=1757\div1760} = U_1(1757\div1760) + U_2(1757\div1760) = 224.4 + 45.6 = 270.0 \pm 6.3$$

corresponding to an increase of 48.6 % thanks to the optimization.

A minimal commentary of the specific characteristics of the optimized layout we presented above is also called for. First of all, we note that the interim solution reached by the program after 1760 epochs is liable to be further improved and is probably not corresponding to a global utility maximum, as also evident by observing the irregular –albeit 120-degree symmetrical by design– pattern of units in the 2-d graph. Still, the radial distribution shows an evident regularity, with three equally spaced peaks at 1250, 2500, and 3750 m from the origin. This indicates that the sets of units clumping at each of the high-density locations on the ground (three clumps at 1250 m radius, 6 at 2500 m, and 6 more at 3750 m) are self-sufficient to "cover" the area surrounding each, which extends by about 1000 m in each direction (the half-side of the equilateral triangle in the center, *e.g.*, is of 1250 m $\times \sqrt{3}/2 = 1082$ m) in all cases. Such a distance scale is at the midpoint between high and low probability to observe a signal, as shown in Fig. 3 (Sec. 4.2).

Another comment concerns the self-organization in clusters. Given 300 macro-tanks, and a requirement that a signal is seen by at least $N_{\text{trigger}} = 10$ macro-tanks for showers to be considered, one would expect that the optimization prefers layouts with clusters populated with a number of units sufficient to guarantee triggering of nearby showers, hence of the order of $15 \div 20$ clusters each populated with $20 \div 15$ macro-units. This is roughly what we observe in the configuration shown in Fig. 15 –15 clusters. The preference for 15 clusters might even be seen as an effect of resiliency to the stochasticity in the way the units drifted to become part of different clusters: with 15 clusters and an average population of 20 units in each, there is a Poisson variability of the order of 4-5 which makes 15-unit clusters still relatively likely (as we do observe) –and that is close to the level at which the probability of triggering starts to be impaired.

We are fully conscious that the above result is highly reliant on the precise definition we decided to investigate for the utility function, and is also liable to change significantly if a different utility is

---

[5]We average the utility values obtained at epochs $0 \div 3$ and $1757 \div 1760$, respectively.
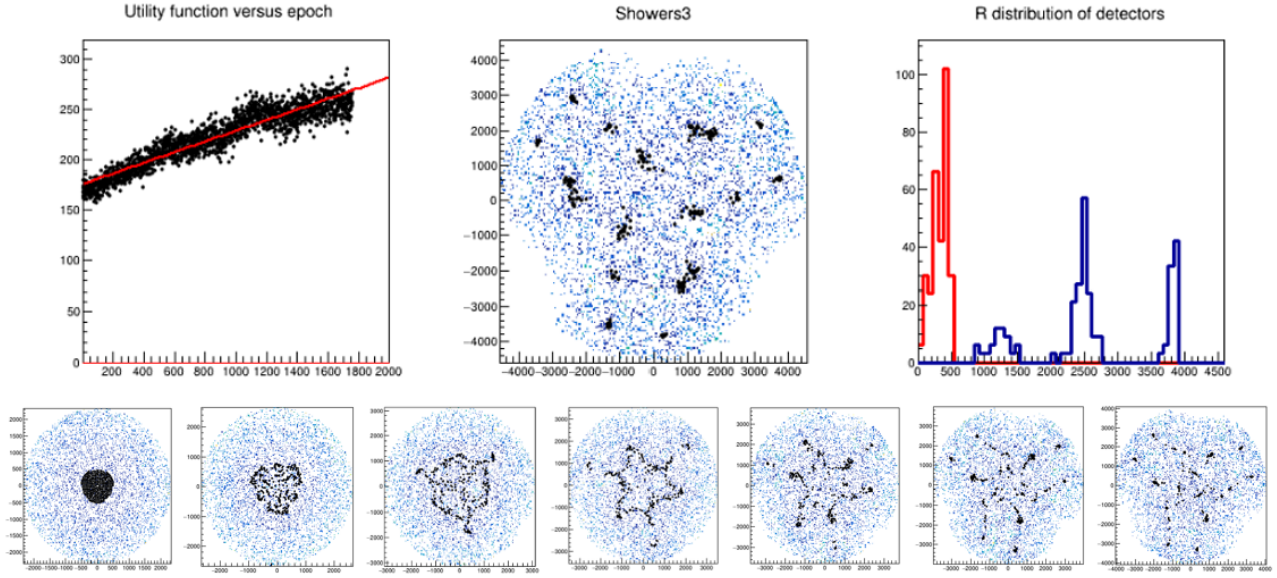
Figure 15: Result of a 1760-epoch optimization run employing 300 19-unit-strong macro tanks, when the utility includes both U_1 and U_2 terms and when showers are generated orthogonally to the ground, and no reconstruction of angular parameters is performed. The graph on the top center shows the best layout after 1760 epochs, and the graph on the top right shows the radial distribution of tanks that correspond to it (in blue) and their initial distribution for epoch 0 (in red). The layouts shown in the bottom row correspond (left to right) to those obtained at epochs 1, 200, 500, 800, 1000, 1200, and 1400.

tested. Still, we point out that the observation is meaningful enough to warrant due attention to the technique we used.

9 Concluding Remarks

In this section we offer a brief summary of the indications we have collected on the layout optimization problem from early tests of the developed software, and a short set of remarks on the future work that ought to be carried out in order to meaningfully exploit it. We are convinced of the importance of these studies, as we have observed very significant variations in the considered utility function as we move from simple-is-best layouts to more contrived, yet cunning, configurations.

9.1 Discussion

If we make no assumptions on the distribution of sources of gamma rays in the sky, we must consider that a ground-based array will be hit by showers from all angles, with a uniform distribution in celestial azimuth and right ascension that translates in a $p(\theta) \propto \sin(\theta)$ polar angle of incidence, and a uniform distribution in azimuthal angle on the ground. The optimal array should therefore, from geometrical considerations alone, have an axial symmetry. However, with a finite number of detection units, a fully symmetric distribution around a point on the plane is not achievable in practice, and one has to consider n-fold angular symmetries as a substitute. This matter seems irrelevant when we consider thousands of detection units, but it constitutes a constraint in an optimization search, and an opportunity to verify the consistency of the identifiable solutions by automated means.

44

In the previous section we have shown how different N-fold symmetries tend to converge to similar arrangements on the ground, but that subtle effects –such as the one arising from the triggering conditions– may influence it in non-trivial ways. We have also observed how the exact specification of the problem, and the details of the reconstruction procedure, have an impact in the determination of the solutions the algorithm converges to. With regards to the dependence on the reconstruction, which is at face value a troublesome feature of what we would like to dress as an end-to-end solution, we note that we have so far considered a sub-optimal, but "legal" setup in our tests, which are preliminary and mainly meant to explore the behavior of the algorithm. A final search of the best solution can only be performed once a full definition of the utility function has been agreed upon, once detailed modeling of the chosen tank characteristics have been coded in the program, and once external constraints (such as total area available for the deployment of the tanks, total number and detailed specification of the tanks) have been considered and included. That is the task that awaits us in the near future.

9.2   Future Prospects

The presented software, while already producing interesting results and offering meaningful suggestions for the placement of the units, requires further improvements before it can become a credible and precise oracle of the final merits of different configurations. We list some of these improvements and shortly comment on them in the list below.

1. Model improvements: as stated above, a number of improvements are possible in the parametric model, and they are liable to have an impact on the performance of reconstruction of the five shower parameters. The improvements include a more precise modeling of the polar angle distribution of primaries, a treatment of disuniformities in the composition of the shower front on the ground, meaningful energy, timing, and angular profiles of the various components of secondaries.

2. Detection units response: depending on the precise choice for the geometry and specification of the tanks, we will be able to introduce in the model a realistic efficiency profile versus angle of incidence and energy of the secondaries, and counting uncertainties at high fluence.

3. Reconstruction method: the likelihood implemented in the current version of the software exploits the full knowledge of the model details, but is liable to be improved both in speed and in accuracy of estimates. Ultimately, we could replace entirely the likelihood reconstruction – and consequently the likelihood ratio test statistic for gamma/hadron separation– by employing a deep neural network; indeed, we have already been developing one such tool, although we are not ready to present results based on it yet.

4. Alternative optimization procedures: the procedure employed in this work –stochastic gradient descent– is a well tested and studied one, but it is not necessarily the most effective for the problem at hand; its shortcomings include the smallness of the gradients that are being used for geometry updates, approximations in the derivation of the density functions of the test statistic employed to gauge the uncertainty on the signal fraction, and other implications, *e. g.* on the need for a fully parametric model. Genetic algorithms are a notable alternative which should be tested; another proposed method consists in starting with an overabundant number of detection units tightly arranged in a wide area, and then proceeding to estimate the quantities of interest by enforcing sparsity in the array by Lasso regression. We plan to consider these alternatives in the near future.

5. Computation of derivatives: Our present approach to compute derivatives analytically is very flexible (e. g. making it easy to operate shortcuts and workarounds for non-differentiable operations) and tangible (making it most obvious to developers which operations are performed on the CPU). The AD approach, which we already employed for testing our derivatives (Sec. 6.3), can be directly used for the derivative computation. When our simulation becomes more and more complex, we expect that AD offers a better scaling of the personpower necessary for creating and maintaining the derivative code.

The success of a high-energy ground-based gamma-ray observatory rests ultimately in a wise set of decisions –on allocation of resources, choice of site, choice of detection units, choice of layout of the units on the ground– that should collectively maximize the desired scientific outputs, once all possible confounding factors, external constraints, detector-related systematic uncertainties have been taken into account. The choice of layout of the detector units is thus only one of many ingredients, but it is also the one which has the loosest coupling to most of the others; it thus offers itself as a good candidate to be studied in isolation, pending the progressive integration of additional factors in the problem. We are convinced that the collaboration ought to work out a baseline definition of a global, experiment-wide utility function which included most if not all the scientific results that are defining its necessity as an addition to the present landscape of running and approved future astroparticle physics experiments. The better specified the global utility will be, the more useful will become all the studies aiming at optimized scientific output.

References

[1] K. Cranmer, J. Brehmer, J. and G. Louppe, *The frontier of simulation-based inference*, Proc. Nat. Acad. Sci. 117, 48 (2020) 30055, arXiv:1911.01429[stat.ML] .

[2] T. Dorigo *et al.*, *Toward the End-to-end Optimization of Particle Physics Instruments with Differentiable Programming*, Rev. in Phys. 10 (2023) 100085, https://doi.org/10.1016/j.revip.2023.100085 .

[3] B. Rossi and K. Greisen, *Cosmic-Ray Theory*, Rev. Mod. Phys. 13, 4 (1941), doi:24010.1103/RevModPhys.13.240 .

[4] A. Tepe, *HAWC: The high altitude water Cherenkov detector*, J. Phys. Conf. Ser. 375 (2012) 052026, 10.1088/1742-6596/375/1/052026 .

[5] Zhen Cao *et al.*, *LHAASO Status and Physics Results*, EPJ Web of Conf. 280 (2023) 01003, 10.1051/epjconf/202328001003 .

[6] A. Aab *et al.*, *The Pierre Auger Cosmic Ray Observatory*, Nucl. Instr. Meth. A 798 (2015) 172, https://doi.org/10.1016/j.nima.2015.06.058 .

[7] B. Bartoli *et al.*, *Calibration of the RPC charge readout in the ARGO-YBJ experiment with the iso-gradient method*, Nucl. Instr. Meth. A 783 (2015) 68, 10.1016/j.nima.2015.02.034

[8] https://www.iap.kit.edu/corsika/

[9] D. Heck, J. Knapp, J.N. Capdevielle, G. Schatz, and T. Thouw, *CORSIKA: a Monte Carlo code to simulate extensive air showers*, https://ui.adsabs.harvard.edu/abs/1998cmcc.book .

[10] See https://www.cnaf.infn.it/en/ .

[11] R.L. Workman *et al.* (Particle Data Group), *Review of Particle Physics*, PTEP (2022) 083C01, 10.1093/ptep/ptac097 .

[12] C.R. Rao, *Information and the accuracy attainable in the estimation of statistical parameters*, Bull. Calcutta Math. Soc. 37 (1945), pp. 81–91. issn: 0008-0659.

[13] D. Kingma and J. Ba, *Adam: A Method for Stochastic Optimization*, arXiv:1412.6980[cs.LG] (2017).

[14] Z. Cao *et al.*, *Ultrahigh-energy photons up to 1.4 petaelectronvolts from 12 γ-ray Galactic sources*, Nature 594, 7861 (2021) 33 doi: 10.1038/s41586-021-03498-z.

[15] M. Aehle, J. Blühdorn, M. Sagebaum, and N.R. Gauger, *Forward-Mode Automatic Differentiation of Compiled Programs*, arXiv:2209.01895 [cs.MS], (2022).